THESIS FOR THE DEGREE OF DOCTOR OF PHILOSOPHY (Ph.D.)

Optimizing Fluorescence Resonance Energy Transfer Measurements

by

Fábián Ákos István, MD

Supervisor: Professor Szöllősi János, PhD, DSC

UNIVERSITY OF DEBRECEN
DOCTORAL SCHOOL OF MOLECULAR MEDICINE

DEBRECEN, 2013

Table of Contents

I. Introduction

The theoretical background of resonance energy transfer was published in 1948 by Förster (1) who described the non-radiative short distance transfer of energy from an excited donor to an acceptor molecule. This process involves simultaneous de-excitation of the donor and excitation of the acceptor molecule. When both donor and acceptor are fluorescent molecules the process is referred to as fluorescence resonance energy transfer (FRET). The rate of energy transfer is inversely proportional to the sixth power of the distance between the donor and acceptor, therefore the efficiency of energy transfer strongly depends on the intermolecular distance of the donor to the acceptor. This distance dependence was exploited by Stryer and Haugland (2,3), who first utilized FRET as a "spectroscopic ruler" to measure the distance between two molecules. With the development of imaging modalities (4-12), FRET was later used to study distance relationships in biological samples (13-16).

Whereas semi-quantitative or qualitative FRET measurements are relatively easy to perform, exact quantitative measurements have not become widespread. First, FRET is influenced by several factors other than the distance between donor and acceptor, which are hard or impossible to control in an experiment. Quantum yield of the donor and relative orientation of the fluorophores are such factors (4,17). A further complicating factor is that FRET theory describes the interaction of one donor with one acceptor (18), whereas most measuring modalities involve ensemble acquisition of the signal of several to hundreds of fluorophores simultaneously. Additionally, in biological samples interaction of one donor with one acceptor is not guaranteed. This can be a result of preexistent uneven protein patterns and distributions or dynamic rearrangements arising from complex formation, protein translocations or simple lateral diffusion in the membrane (19-21). Additionally, when fluorescently tagged antibodies are used, usually multiple fluorophores are coupled to an antibody to achieve better signal-to-noise ratios. We therefore sought to investigate how measured transfer efficiency is influenced by multiple interacting fluorophores. This was achieved by varying the fluorophore-to-protein (F/P) ratio of fluorescently labeled antibodies and observing the changes in FRET efficiency in an intramolecular model system.

Originally, FRET was limited to viewing the interaction between one donor and one acceptor species. However, in the early 2000's it was realized that the addition of a third dye could

expand the capabilities of traditional FRET measurements (22). First of all, functioning as a relay point, the third dye increased the interaction range that could be viewed with FRET. Secondly, the third dye allowed FRET to be viewed between three distinct molecular species, so that the relative orientation of three molecules could be assessed at the same time. This has significant potential for biological investigations, where higher order multimers and multi-component signaling complexes play important roles in governing biological function. While providing significant gains, the addition of a third dye also presents several problems. Instrumentation requirements increase, as the instrument of choice has to be able to detect and excite three different fluorophores while at the same time allowing separation of the individual signals. The theory of FRET in a three-dye system is exceedingly more complex than in a two-dye system, resulting in more extensive calculation requirements. Several methods have been developed to measure FRET in a three-dye system. However, the complexity of the three dye system required simplification, either through extensive sample preparation, restricted sample selection or neglecting of transfer routes. We therefore developed a new method – tripleFRET – that can be implemented with a broad range of biological samples and does not require specific sample preparation beyond fluorescent labeling.

II. Literature review

1. Applications of FRET

Energy transfer measurements have become widespread in the last decade, with FRET methods being applied to answer a large variety of scientific questions. A current search for the phrase "FRET" on PubMed will yield almost 6000 results, showing the immense body of work that is involved. Important scientific discoveries were made in several areas of cell biology. FRET measurements were successfully applied to investigate how lipid anchors determine subcellular localization of proteins to lipid rafts (23). A lifetime imaging based FRET technique helped verify ligand-independent lateral propagation of receptor signaling after focal stimulation of ErbB1 with EGF (24). Several steps in B cell antigen receptor (BCR) (25) and T cell antigen receptor (TCR) activation (26) were elucidated with FRET measurements. Conformational change (27-30) and oligomerization of proteins (31-33) was also visualized with FRET. Different FRET constructs have been successfully employed as biosensors to monitor protein kinase (34,35) and GTP-binding protein activation (36), small GTPase (37) and HIV-1 protease activity (38). FRET has also been effectively combined with PCR methods to increase speed and precision of detection (39-41).

Our own department has used FRET extensively in its research. With the help of FRET:

- assembly of interleukin 2 subunits on the T cell surface was investigated (42);
- co-clustering of HLA class I and II molecules was visualized on lymphoblastoid cells (43);
- EGF induced redistribution of ErbB2 on breast tumor cells was characterized (13);
- FRET data was used to construct a three dimensional model of a supramolecular cluster containing HLA class I, TCR and CD8 molecules (44);
- CD45 isoforms were shown to differentially associate with CD4 and CD8 and regulate TCR signal transduction on T lymphocytes (45);
- hetero- and homoassociation of ErbB proteins on the cell surface of breast cancer cells was characterized (46);
- supramolecular receptor clusters of IL-2 and IL-15 receptor α-, β- and γ-subunits as well as MHC class I and II glycoproteins were identified in lipid rafts of T cells (21);

- FRET data was used for molecular modeling of the ErbB2 receptor (47);
- association of ErbB2, β1-integrin and lipid rafts was investigated on breast and gastric tumor cell lines (48);
- large-scale association of ErbB1 and ErbB2 was characterized with a homo-FRET study (20);
- initial attempts were also made to expand the FRET system to monitor the interaction of three molecules with a two-sided FRET approach (49).

In summary, FRET experiments have become ubiquitous, with diverse methods for microscopic or flow cytometric setups (9,11,12,16). The newer methods are able to harness the potential of fluorescent proteins (50-54) and high through-put methods are also emerging (8,55-58), making FRET measurements a diverse tool to tackle scientific questions of the nanometer distance range.

2. Theory of FRET

Fluorescence resonance energy transfer (FRET) is a non-radiative energy transfer process, in which an excited donor molecule excites an adequately oriented fluorescent acceptor molecule via a long distance (1-10 nm) dipole-dipole interaction (1). Transfer efficiency, which is the probability that a donor excitation quantum is transferred to an acceptor, is given as:

$$E = \frac{k_{transfer}}{k_{transfer} + k_{other}} \tag{1}$$

where $k_{transfer}$ is the rate constant of energy transfer and k_{other} is the sum of the rate constants of all other de-excitation pathways. The rate of transfer is determined by the distance between the donor and acceptor as follows:

$$k_{transfer} = k_{other} \cdot \left(\frac{R_0}{r} \right)^6 \tag{2}$$

where r is the separation of the donor and acceptor and R_0 is the so called Förster distance characteristic for the donor-acceptor pair. The Förster distance is a function of the spectral characteristics of the dyes used and can be calculated as:

$$R_0 = 978 \cdot \left(Q_D \kappa^2 n^{-4} J_{DA} \right)^{1/6} \tag{3}$$

where Q_D is the donor quantum yield in the absence of acceptor dyes, κ^2 is an orientation factor (its value can range from 0 to 4 and is $^2/_3$ for dynamically averaged isotropic transition moments (59)), n is the refractive index of the conveying medium and J_{DA} is the spectral overlap integral of the donor emission and acceptor excitation spectra (without this spectral overlap energy transfer cannot occur). After combining equations (1) and (2), we arrive at the following form for transfer efficiency:

$$E = \frac{1}{1+\frac{r^6}{R_0^6}} \tag{4}$$

Therefore the Förster distance corresponds to the distance at which the transfer efficiency between donor and acceptor is 50%. This distance dependence makes FRET efficiency a sensitive indicator of intermolecular distance (Figure 1).

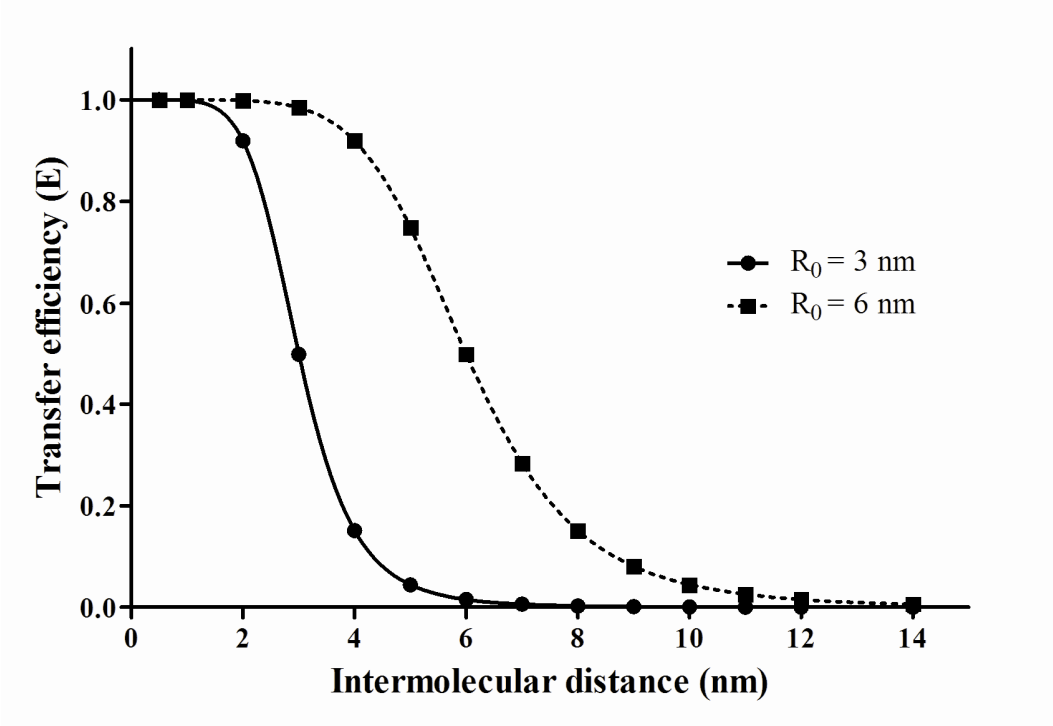

Figure 1. Distance dependence of transfer efficiency at different R_0 values

3. Methods to measure FRET

The presence of FRET alters the apparent properties of the dyes investigated. These spectral changes can be measured to determine FRET. We can divide the methods into intensity-based

methods (which rely on detecting changes in the quantitative emission of the donor and/or the acceptor) and lifetime-based methods.

a) Intensity-based methods

Due to FRET, excitation energy of the donor is transferred to the acceptor. This results in quenching of donor intensity and simultaneous sensitized emission (emission without direct excitation from an external light source) of the acceptor. Several methods exist that exploit these phenomena. The simplest method involves measuring donor fluorescence intensity alone and in the presence of an acceptor (60,61). If F_D is the intensity of the sample labeled only with donor and F_{DA} is the intensity of the sample labeled with donor and acceptor, then transfer efficiency can be calculated as:

$$E = 1 - \frac{F_{DA}}{F_D} \tag{5}$$

This method has the drawback that two separate samples are required; therefore changes in expression levels or antibody binding affinity between samples can skew results. The advantage is that one detection channel and one excitation wavelength is sufficient for transfer efficiency measurement. The method can be used both in microscopy and flow cytometry.

A more complex method is the so called acceptor photobleaching (abFRET) method (62-64). The method involves measuring donor intensity before and after irreversible destruction of the acceptor with a high intensity excitation light source (hence the term photobleaching). Transfer efficiency is determined from the following equation:

$$E = 1 - \frac{F_{BB}}{F_{AB}} \tag{6}$$

where F_{BB} and F_{AB} are the donor intensity before and after bleaching, respectively. Problems can arise from partial bleaching of the donor during the acceptor photobleaching step, the production of so called dark acceptors (non-fluorescent acceptors generated from bleaching of acceptors; these acceptors may quench donor emission even after apparent loss of acceptor emission) and generation of fluorescent acceptor degradation products that mimic the emission profile of the donor (65). The time required for photobleaching renders this method impractical for use with flow cytometers and photobleached regions or samples cannot be re-measured once imaged.

The intensity-based method can be further refined by simultaneously detecting quenched donor emission and sensitized acceptor emission (9,12). In a consecutive imaging step, directly excited acceptor emission is also measured. Altogether three intensity channels are detected: I_1 ─ excitation at donor wavelength and donor emission filter (donor channel); I_2 ─ excitation at donor wavelength and acceptor emission filter (energy transfer channel); I_3 ─ excitation at acceptor wavelength and acceptor emission filter (acceptor channel). With these three intensities the following initial equation set can be given:

$$\begin{aligned} I_1 &= I_D\left(1-E\right)+S_4 I_A \\ I_2 &= S_1 I_D\left(1-E\right)+S_2 I_A + I_D E\alpha \\ I_3 &= S_3 I_D\left(1-E\right)+I_A \end{aligned} \tag{7}$$

where I_D and I_A are the unquenched donor intensity and pure acceptor intensity respectively, E is the transfer efficiency, S_1–S_4 are correction factors for cross-excitation and spectral spillover determined from donor-only and acceptor-only labeled samples:

$$\begin{aligned} S_1 &= \frac{I_2^D}{I_1^D} \qquad & S_2 &= \frac{I_2^A}{I_3^A} \\ S_3 &= \frac{I_3^D}{I_1^D} \qquad & S_4 &= \frac{I_1^A}{I_3^A} \end{aligned} \tag{8}$$

where upper indices signify whether samples labeled only with the donor dye (D) or with only the acceptor dye (A) are measured. The alpha factor is a scaling factor correcting for the difference in the fluorescence quantum yields and detection efficiencies of donor and acceptor fluorophores. Basically, the alpha factor can be considered as a "currency exchange rate" to scale loss of donor emission to gain of acceptor emission. The alpha factor can be determined empirically from the following formula:

$$\alpha = \frac{I_2^A}{I_1^D} \cdot \frac{L_D B_D \varepsilon_D}{L_A B_A \varepsilon_A} \tag{9}$$

where $I_2{}^A$ is the I_2 signal of acceptor-only labeled sample and $I_1{}^D$ is the I_1 signal of donor-only labeled sample, L is the labeling ratio of the antibodies, B is the mean number of receptors labeled, and ε is the molar excitation coefficient of the dyes at the donor excitation wavelength (the D and A indexes refer to donor and acceptor, respectively). The ratio of molar extinction

coefficients of the fluorophores at the donor excitation wavelength ($\varepsilon_D/\varepsilon_A$) is the so-called *efr* coefficient. Solving of equation (7) yields the following term:

$$A = \frac{E}{1-E} = \frac{I_2 - S_1 I_1 + (S_1 S_4 - S_2) I_3}{\alpha (I_1 - S_4 I_3)} \tag{10}$$

From this transfer efficiency is calculated as:

$$E = \frac{A}{1+A} \tag{11}$$

The method can be used in microscopy and flow cytometry as well.

A further method relying on emission profiles is the so called spectral un-mixing method (51,52,54,66). When the emission spectra of donor and acceptor show significant overlap (as is often the case with fluorescent proteins), separation of emission signals with traditional band- and longpass filters can be impractical. The difficulty lies in finding a filter that is exclusive (i.e. the majority of the intensity signal originates from one fluorophore) and still allows for a good signal-to-noise ratio.

In spectral unmixing, the combined emission of fluorophores is detected in multiple channels (usually at least four). The characteristic emission spectrum of each fluorophore as seen by the detector array is recorded before hand and can be used as a reference that relates the signal amplitude of the fluorophore in every detection channel. In the FRET sample, emission intensity in any given detection channel is determined by the contribution from both fluorophores. With a proper deconvolution algorithm the intensity signal of each fluorophore can be "linearly unmixed" based on the characteristic emission spectrum and a relative abundance factor that is shared between channels. The unperturbed fluorophore intensity acquired in such a fashion can then be used for transfer efficiency measurements. Recently, spectral imaging has been achieved with flow cytometers as well; however FRET implementation has been only published for microscopy.

b) Donor photobleaching

Photobleaching involves irreversible photochemical degradation of excited fluorophores. Since photobleaching requires the fluorophore to be in the excited state, every process that decreases the average time spent in the excited state will consecutively reduce the probability of photobleaching and increase the bleaching decay constant (16,67,68). Energy transfer as an alternative de-excitation route increases evacuation of the excited state and slows the bleaching

of the donor. The bleaching time constants for the donor in the absence (τ_D) and presence of acceptor (τ_{DA}) can be written as:

$$\tau_D = \frac{k_{other}}{k_{exc}k_{bleach}}$$
$$\tau_{DA} = \frac{k_{transfer} + k_{other}}{k_{exc}k_{bleach}} \quad (12)$$

where k_{other} is the sum of the rate constants of all de-excitation pathways except for energy transfer and k_{exc}, k_{bleach} and $k_{transfer}$ are the rate constants of excitation, photobleaching and energy transfer, respectively. For energy transfer measurements, an image sequence has to be recorded for both donor only and donor-acceptor labeled samples. The intensity-time curves are fitted to determine the fluorescence intensity decay time constants. Energy transfer is calculated as:

$$E = 1 - \frac{\tau_D}{\tau_{DA}} \quad (13)$$

In cellular imaging studies, the time required for photobleaching renders this method effective only in microscopy.

c) Fluorescence lifetime methods

The flurescence lifetime describes the average time a fluorescent molecule spends in the excited state and is the reciprocal of the sum of the rate constants of all de-excitation processes:

$$\tau = \frac{1}{k_{de-excitation}} \quad (14)$$

Fluorescence lifetime imaging microscopy was developed in the early 1990's (33) and allows the determination of fluorescence lifetimes of biological samples in a microscope. The fluorescence lifetime of a sample can be measured either in the time domain with a short, pulsed excitation beam or through phase modulation (69). FRET as an additional de-excitation process shortens the time spent in the excited state and therefore the fluorescence lifetime as well. The fluorescence lifetimes of the donor alone (τ_D) or in the presence of an acceptor (τ_{DA}) can be written as:

$$\tau_D = \frac{1}{k_{other}}$$
$$\tau_{DA} = \frac{1}{k_{other} + k_{transfer}} \quad (15)$$

where $k_{transfer}$ is the rate constant of energy transfer and k_{other} is the sum of the rate constants of all other de-excitation pathways. The expression for transfer efficiency then is:

$$E = 1 - \frac{\tau_{DA}}{\tau_D} \quad (16)$$

Given proper measurement accuracy and fitting algorithms, both donor only and FRET shortened lifetimes can be measured from the same sample, therefore samples in FLIM-FRET experiments do not require external controls.

4. Apparent energy transfer efficiency

The theory of transfer efficiency states that the measured transfer efficiency for a given donor-acceptor pair at a given distance depends on the separation of donor and acceptor and the Förster distance of the dye pair. Since the Förster distance is a function of the spectral characteristics of the dye pair and of orientation- and conveying medium dependent factors (which are approximated to be stable), changes in transfer efficiency should mirror changes in donor-acceptor distance. This molecular level transfer efficiency of a given dye pair can be referred to as true or characteristic transfer efficiency and harbors actual distance information. However, the actual measured transfer efficiency in a given FRET experiment may not accurately reproduce the true transfer efficiency. One way this can occur is when multiple fluorophores are measured simultaneously. In this case the emissions from all fluorophores are detected, so that signals from different populations are averaged (70). The energy transfer for the measured population is:

$$E = \sum_{i=1}^{n} d_i E_i \quad (17)$$

where E_i is the characteristic transfer efficiency of the *ith* donor-acceptor population and d_i is the fraction of the *ith* population to the total donor-acceptor population. Basically, the measured transfer efficiency will be the weighted average of populations with different characteristic transfer efficiencies, where the weighting factor is the relative contribution of each population to

the total population. In the simplest form, the donor population can be divided into un-paired donors without a suitable acceptor within energy transfer range and donors paired with acceptors for energy transfer (71). In this case measured transfer efficiency will be smaller than the characteristic transfer efficiency, since the FRET signal of paired donors is offset by the non-transfer signal of un-paired donors. This effect is only true for the measurement methods that detect intensity signals from multiple fluorophores simultaneously; therefore single molecule methods are not affected. The methods relying on fluorescence lifetime are also not affected, since the peaks of lifetime distributions are not shifted by relative population contribution. The main concern is that for ensemble intensity-based measurements (which require the least specific instrumentation and simplest calculations and are therefore the most widespread methods), apparent FRET cannot be equated with intermolecular distance if the contribution of different populations is not known. Also, apparent FRET can be influenced by shifts in association patterns without actual intermolecular distance changes.

The Förster equations dictate that transfer efficiency is the ratio of the rate constant of de-excitation through energy transfer to the sum of the rate constants of all forms of de-excitation (see equation (1)). Multiple acceptors interacting simultaneously with the same donor will increase the rate constant of energy transfer (4,72-75) in a manner that is independent of the factors in equation (2). This results in increased transfer efficiency without closer proximity between donor and acceptor. Therefore, distance calculations based on the R_0 derived from equation (3) will be inaccurate, since it only applies for the case of interaction of one donor with one acceptor (4,18). This effect is taken into consideration when measuring transfer efficiency of freely moving fluorophores in a two dimensional plane (74) or energy transfer between a plane of acceptors and a donor above the plane. In these cases special modeling and calibration schemes have to be applied to accurately determine interdye distances (47,76,77). Similarly, it has been shown, that an increase in number of acceptor fluorophores increases transfer efficiency measured for fluorescent protein constructs (75). Since the effect of multiple acceptors interacting with a single donor is realized at the level of rate constants, all methods for measuring FRET will report increased apparent transfer efficiency as compared to the case of interaction between one donor and one acceptor.

5. Theoretical background of three-dye FRET

The theoretical groundwork of three-dye FRET systems was published by Watrob *et al* in 2003 (22) and describes the different energy transfer routes that occur in such a system (Figure 2). Briefly, if the three dyes are designated with increasing excitation wavelength as dye A, B and C, the following behavior can be observed: the dye with the shortest excitation wavelength – dye A – is the global energy donor for dyes B and C; the dye with the intermediate excitation wavelength – dye B – is an acceptor for dye A and a donor for dye C; the dye with the longest excitation wavelength – dye C – is a global acceptor. Regarding the total transfer of energy from dye A to C, two main cases are distinguished (see also Figure 2): in the first a direct, one-step FRET occurs between A and C (E_{AC}); in the second an indirect, two-step FRET occurs, where energy is first transferred from A to B (E_{AB}) and then from B to C (E_{BC}). The latter sequence is also called relay-FRET. Since relay-FRET arises from two independent excitation─de-excitation processes, it can be written as:

$$E_{relay} = E_{AB} \cdot E_{BC} \tag{18}$$

In this case dye B functions as a "relay post", increasing the total energy transferred from dye A to C. When direct transfer can occur from dye A to B and from dye A to C as well, the two acceptors compete for the same donor. This has the consequence that instead of the original non-competitive energy transfers (E_{AB}, E_{AC}), apparent competitive energy transfers are measured (E'_{AB}, E'_{AC}). The relationship between the competitive and non-competitive energy transfers can be calculated as:

$$\frac{E'_{AB}}{E_{AB}} = \frac{k_{AB}}{k_{AB}+k_{AC}+k_{other}} \frac{k_{AB}+k_{other}}{k_{AB}} = \frac{k_{AB}+k_{other}+k_{AC}-k_{AC}}{k_{AB}+k_{AC}+k_{other}} = 1-E'_{AC} \tag{19}$$

$$\begin{aligned} E'_{AB} &= E_{AB}\left(1-E'_{AC}\right) \\ E'_{AC} &= E_{AC}\left(1-E'_{AB}\right) \end{aligned} \tag{20}$$

$$\begin{aligned} E_{AB} &= \frac{E'_{AB}}{\left(1-E'_{AC}\right)} \\ E_{AC} &= \frac{E'_{AC}}{\left(1-E'_{AB}\right)} \end{aligned} \tag{21}$$

Naturally, direct and relay-FRET can occur at the same time. In this case the total energy transfer from dye A to C (E_{total}) is:

$$E_{total} = E_{relay} + E'_{AC} = E'_{AB} \cdot E_{BC} + E'_{AC} \quad (22)$$

While this description of a three-dye system is didactically straight forward, as we shall later discuss, the actual behavior of the imaged dyes in three-dye FRET studies does not necessarily adhere to just one of the main cases. Different dye populations can follow different interaction schemes and one dye can be a component of several transfer schemes simultaneously (of course with different interaction partners). This alone can make interpretation of real world measurements in three-dye systems difficult.

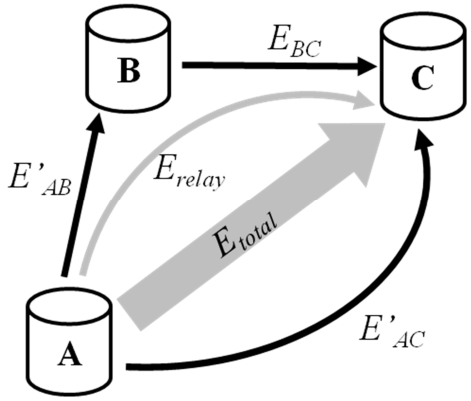

Figure 2. Schematic drawing of a three-dye system with possible energy transfer routes. E'_{AB} and E'_{AC} values refer to transfer efficiencies measured in the presence of competition between transfer processes from A to B and A to C. $E_{relay} = E'_{AB} \cdot E_{BC}$ is the transfer efficiency between A and C via B, $E_{total} = E'_{AC} + E_{relay}$ is the total probability of energy transfer from A to C via the direct and indirect mechanisms.

6. FRET studies in three-dye systems

Theoretically the use of three-dye FRET systems presents an excellent tool to investigate interactions of multi-molecule systems and molecular level conformational changes. However, detecting the emission of three dyes simultaneously makes it difficult to separate the undistorted FRET signals and measure energy transfer quantitatively. Several workarounds exist that still allow harnessing additional information from three component FRET systems without having to dissect the complex emission profiles. One approach involves using sequential imaging, where first an acceptor photobleaching is performed to measure FRET from dye B to C and then in a second step donor photobleaching to measure FRET from dye A to B (49). The acceptor photobleaching step - by bleaching dye C - liberates dye B from quenching and does not influence the consecutive donor photobleaching step. While this method does not allow assessing direct transfer from dye A to C or relay-FRET, it allows pair wise co-localization studies and

distance measurements of cell-surface proteins. The measurement of energy transfer between dye B and C is not influenced by the third dye. Therefore quantitative evaluation of transfer from dye B to C is possible even if transfer from dye A to B and dye A to C is only determined qualitatively or semi-quantitatively. Ernst *et al* employed this approach to monitor function of the F_0F_1-ATP synthase and elastic deformations within the rotary unit during ATP hydrolysis (78). Finally, elimination of one fluorophore altogether can be achieved with bimolecular fluorescence complementation (BiFC) FRET (79). Briefly, BiFC involves labeling two molecules of interest with complementary fragments of a fluorescent protein. If the two molecules are in close interaction a functional fluorescent protein is produced and characteristic fluorescence emission can be detected. A third molecule can be labeled with an appropriate fluorescent dye for FRET experiments. Therefore, in BiFC FRET measurements energy transfer only occurs when all three molecules of interest are in close proximity of each other.

Full-fledged attempts at three-dye FRET are relatively sparse. Initial studies focused on verifying three-dye FRET as a feasible tool to investigate biomolecules, with DNA strands as the molecule of choice (22,80,81). The advantage of DNA strands is that the distance between fluorophore binding places (usually a hybridization probe is used) can be precisely controlled by varying the number of nucleotides in between. The rigid DNA strands have the additional advantage of limiting possible spatial distributions of the fluorophores to discrete relative positions. This simplifies the interaction scheme and allows easier energy transfer measurements. Liu *et al* utilized a three-dye system to monitor branch movements of a DNAzyme and metal-ion-dependent conformational changes (82). They employed a ratiometric method similar to the donor quenching method in two-dye systems. Conformational changes of DNA Holliday junctions were monitored with a single-molecule three-dye technique, which used a simplified approach of the three-dye FRET matrix (83). The Holliday junction was also the complex of choice for the investigations of Lee *et al*, who employed a microscope-based ratiometric method (84). Galperin *et al* successfully verified that a three-dye FRET method was also applicable to fluorescent protein constructs in vitro (85). Both a ratiometric intensity-based approach and a method relying on donor fluorescence recovery after acceptor photobleaching (DFRAP) were used. DFRAP involves selective photobleaching of an acceptor and observing the increase in donor fluorescence after the loss of quenching from the acceptor. The group successfully identified Rab5 interaction with early endosomal antigens and activation complexes of epidermal

growth factor receptor, Grb2 and Cbl. Later, a semi-quantitative donor quenching method showed in vivo TRAF2 (tumor necrosis factor receptor-associated receptor 2) trimerization (86). Lee *et al* used a DNA system to successfully sort triple-labeled DNA strands with different intra-strand dye distances (87). They then monitored movement of RNAP during translocation along a DNA strand. The relay function of the intermediate dye was demonstrated by Aneja *et al* in experiments using cationic conjugated polymer (CCP), fluorescein and tetramethylrhodamine (TAMRA) (88). An increase in sensitized TAMRA emission was observed after adding fluorescein to a CCP-TAMRA FRET system. A similar study was also carried out using DNA thin films (89). Most recently, several techniques are emerging for detecting FRET in four dye systems (90-92), however even the simpler three-dye methods have not become widespread, chiefly because of unique instrumentation and sample preparation requirements.

III. Scientific goals of the thesis

The apparent FRET is influenced by the number of interacting partners. This effect has relevance in biological studies, since activation and movement of proteins can lead to formation of complexes and aggregates with several components within energy transfer range. Also, for fluorescent studies, several fluorophores are tagged to labeling molecules to enhance brightness and increase the signal-to-noise ratio. To determine the effect on transfer efficiency of multiple fluorophores interacting simultaneously, we used an intramolecular FRET system and varied the fluorophore-to-protein (F/P) ratio of the antibodies used. We had three main goals:

- Determine the behavior of different F/P ratio variants of antibodies with respect to intensity and cellular affinity.
- Determine how the interacting number of acceptors influences transfer efficiency.
- Determine how the interacting number of donors influences transfer efficiency.

Previously, three-dye FRET methods were restricted to either semi-quantitative efficiency determination or neglected transfer processes to facilitate interpretation of FRET signals. Permutations of donor quenching were used mostly, necessitating an external reference sample to determine unquenched donor emission. To circumvent these shortcomings, we had the following objectives:

- Lay down the mathematical background for a three-dye intensity-based method that allows computation of direct individual FRET between dyes A, B and C as well as relay- and total-FRET without a reference sample.
- Verify the method with a three-dye labeling scheme of cell-surface proteins and compare results with those obtained with conventional two-dye intensity-based FRET.
- Evaluate the method on molecular systems with variable interacting schemes.

IV. Materials and Methods

1. Cell lines

Human gastric cell line NCI-N87 with high ErbB2 (member of the epidermal growth factor receptor family) and major histocompatibility complex (MHC) class I expression level (48) was obtained from the American Type Culture Collection (Rockville, MD, USA) and grown according to the manufacturer's specification (in RPMI containing 10% fetal bovine serum, 2 mM L-glutamine, and 0.25% gentamicin in 5% CO_2 atmosphere) to confluency. For flow cytometry, cells were harvested by treatment with 0.05% trypsin and 0.02% ethylenediamine-tetraacetic acid before antibody labeling.

2. Conjugation of antibodies with fluorescent dyes

In our experiments we used the following anti-ErbB2 monoclonal antibodies (mAbs): pertuzumab (a gift from Hoffman-La Roche, Grenzach-Wyhlen, Germany); trastuzumab (purchased from Hoffman-La Roche, Grenzach-Wyhlen, Germany); and H76.5 antibody (prepared from the hybridoma cell line, a kind gift of Yosef Yarden). An approximate epitope map of the antibodies used is shown in Figure 3. Covalent binding of the monofunctional succinimidyl ester derivates of amine-reactive dyes (Alexa Fluor 488, Alexa Fluor 546, Alexa Fluor 555 and Alexa Fluor 647; Molecular Probes/Invitrogen, Eugene, OR, USA) to the lysyl-ε amino groups of antibodies was carried out in 0.1 M sodium bicarbonate buffer at pH 8.3. Dyes dissolved in sodium bicarbonate buffer were added to antibody solutions, and the reaction mixture was incubated at room temperature for 1 hour. Unreacted dye molecules were removed by gel filtration through a Sephadex G-50 column. To achieve different fluorophore-to-protein (F/P) ratio of the antibodies we changed antibody concentration, pH and/or labeling time.

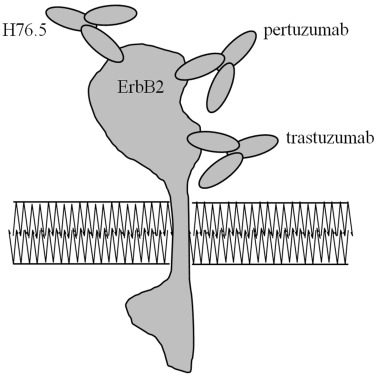

Figure 3. Approximate epitope map of antibodies used for labeling ErbB2. Antibody size is approximately 145 kDa, ErbB2 size is 185 kDa.

The F/P labeling ratio was determined from absorption at 280 nm and the maximum absorption wavelength of the dye used by spectrophotometry (Nanodrop, Wilmington, DE, USA) and was in the range of 1–10 for whole mAbs. In order to prevent artifact production and remove aggregates, dye-conjugated mAbs were fuged in the cold (4°C) at 110,000 × *g*, for 20 min in an Airfuge ultracentrifuge (Beckman Coulter, Fullerton, CA, USA) before cell labeling. Production of different F/P ratio variants and measurement of F/P ratio was performed by Rente Tünde.

3. Labeling cells with fluorescent antibodies

For flow cytometry, freshly harvested cells were washed twice in ice-cold phosphate buffered saline (PBS; pH 7.4). The cell pellet was suspended in PBS at a concentration of 2×10^7 cells/ml. Then 25 µl of conjugated antibodies were added to 25 µl of cell suspension and cells were incubated for 30 min on ice. The excess of antibody was at least fivefold above saturating concentration (final labeling concentration of 100 μg/mL) during the incubation. Thereafter cells were washed twice in PBS and fixed in 500 μL of 1% formaldehyde-PBS. During labeling special care was taken to keep the cells at ice-cold temperature to avoid induced aggregation of cell surface molecules. Labeling of cells for experiments with different F/P ratio antibody variants was performed by Rente Tünde.

4. Instrumentation and sample measurement

For experiments to determine the effects of multiple FRET partners interacting simultaneously, measurements were carried out on a FACSArray bioanalyzer (Becton Dickinson, Franklin Lakes, NJ, USA). The flow cytometer is equipped with a 532-nm solid-state laser and a 635-nm diode laser, and for FRET measurements the detectors with 585/42 band pass (donor channel; I_1), 685 long pass (energy transfer channel; I_2), and 661/16 band pass (acceptor channel; I_3) filters were used. For every sample 20,000 events were acquired.

For tripleFRET measurements, we used a FACSVantage SE with DiVa option flow cytometer (Becton Dickinson, Franklin Lakes, NJ, USA) equipped with a 488-nm water-cooled Argon-ion laser, a 532-nm diode pumped solid-state laser and a 633-nm air-cooled HeNe laser. The fluorescence detection channels (emission filters and laser wavelengths used for excitation) for the three fluorophores are shown in Table 1.

Table 1
Laser excitation wavelengths and emission filters of intensity channels for tripleFRET

Channel	Laser wavelength (nm)	Filter
I_1	488	530/30
I_2	488	585/42
I_3	488	675/20
I_4	532	585/42
I_5	532	650 LP
I_6	633	650 LP

Band pass ranges are given as full width at half maximum (FWHM) values.

5. Evaluation of transfer efficiency

For all FRET experiments, manual gating was performed on the FSC – SSC plot to exclude debris and doublets. Samples labeled with one dye only were used to determine non-specific background corrected intensities in native dye channels. In two-dye systems double-positive populations were gated and used for FRET calculations. For tripleFRET measurements double-positive populations were gated in the triple-labeled sample. Populations either positive for dye A and B or positive for dye A and C were gated. The intersection of the two populations gave a population that is positive for dyes A, B and C. This population was used for tripleFRET analysis. Transfer efficiency histograms were generated for all possible FRET processes, and after manual gating the value of median transfer efficiency was determined.

To evaluate FRET data obtained with flow cytometry, ReFlex software (free-ware, available at http://www.freewebs.com/cytoflex) was used with the equations entered in the equation editor of the program (93). Intensity-based FRET for two-dye systems was calculated according to the equation set (7). In our setup S3 and S4 were negligible, therefore a modified form of equation (10) was used:

$$A = \frac{E}{1-E} = \frac{1}{\alpha} \cdot \frac{I_2 - I_1 S_1 - I_3 S_2}{I_1} \qquad (23)$$

For tripleFRET measurements the equation set introduced in the Results section of this thesis was used. Transfer efficiency values are given as median values of transfer efficiency histograms. Flow cytometric dotplots and histograms were generated with ReFlex, three-dimensional transfer efficiency scatter plots were created with Wolfram Mathematica 7 (Wolfram Research, Champaign, IL, USA).

6. Determining alpha-, cross-excitation- and spillover-factors

Since alpha factors are scaling factors correcting for the difference in the fluorescence quantum yields and detection efficiencies of donor and acceptor fluorophores, the intensity of the same number of excited donor and acceptor fluorophores has to be measured at given wavelengths. This is most easily done by labeling a cell-surface protein with donor- and acceptor-tagged antibodies in separate samples. Alternatively, two different antibodies can be used that do not compete with each other for binding and that recognize epitopes far enough apart so that energy transfer does not occur (12,94). Another possibility is to apply epitopes with known distances and well characterized transfer efficiencies, and set the value of alpha to yield the reference transfer efficiencies (12). When using fluorescent proteins, donor-acceptor fusion proteins can be constructed where the expression level of both fluorophores are the same. By varying the length of the linker region (53) or by using an iterative method yielding E and alpha simultaneously (95), alpha can be calculated. For our experiments, the average intensity of several thousand cells singularly labeled with Alexa Fluor 488, Alexa Fluor 546, Alexa Fluor 555 or Alexa Fluor 647 was used for the calculation of alpha factors according to equations (9) and (30). Cross-excitation and spillover factors were measured on single-labeled samples. For two-dye intensity-based FRET calculations, *S*-factors were calculated according to equation (8). For tripleFRET measurements, *S*-factors were determined according to equation (29).

7. Anisotropy measurements

Fluorescence anisotropy measurements were performed on a Fluorolog-3 spectrofluorimeter (Horiba Jobin Yvon, Longjumeau, France). The excitation light was provided by a 450-W Xe-arc lamp. Anisotropy of Alexa Fluor 546, -555 and -647 conjugated trastuzumab, free dye solutions and PBS solution were measured with FL-1044 polarizers in L-format configuration. The concentration of the fluorescent conjugated antibodies and free dyes were in the range of 10^{-7}–10^{-6} M, where absorption of the sample was below 0.05 to ensure negligible inner filter effects. A 1 cm optical pathlength quartz cuvette (Hellma, Müllheim, Germany) was used. Excitation and emission monochromator wavelengths were set according to emission and excitation maxima of the dyes applied. Slit width and acquisition time were chosen so that all polarizer-mode intensities (I_{VV}, I_{VH}, I_{HH} and I_{HV}) for all concentrations remained below

1,000,000 counts per second. Data were analyzed with DataMax for Windows v2.1 software. Sample preparation for anisotropy measurements was performed by Rente Tünde.

8. Pearson's correlation coefficient

The Pearson's correlation coefficient introduced in the Results section can be calculated as:

$$r = \frac{\sum_{i=1}^{n}\left(x_i - \bar{x}\right)\left(y_i - \bar{y}\right)}{\sqrt{\sum_{i=1}^{n}\left(x_i - \bar{x}\right)^2}\sqrt{\sum_{i=1}^{n}\left(y_i - \bar{y}\right)^2}},$$

and quantifies the linear relationship between x and y variables of a data set. The range of r is between -1 and 1, where 1 is the perfect linear relationship.

V. Results

1. Determining the effect of multiple FRET partners interacting simultaneously

The effect of fluorophore abundance was determined by measuring energy transfer with different fluorophore-to-protein (F/P) ratio versions of the same antibodies. This way the ratio of donors to acceptors could be easily controlled through the F/P ratio of the antibodies used. Changing F/P ratios does not influence biological behavior (different F/P ratio variants of the same antibody will have the same biological effect), therefore differences in transfer efficiency will be a consequence of altered F/P ratio and not an uncontrolled biological factor.

We measured the energy transfer between fluorescently conjugated pertuzumab and trastuzumab (96,97) targeted against ErbB2 (98) cell surface proteins on NCI-N87 cells (99). The expression level of ErbB2 on NCI-N87 cells is high ($8 \times 10^5 – 10^6$ /cell) (100), allowing good detection sensitivity. The energy transfer between the two antibodies can be readily detected and is often used as a positive control by our workgroup. The FRET between trastuzumab and pertuzumab can be regarded as a primarily fixed distance intramolecular energy transfer within the same ErbB2 protein (13), therefore changes in transfer efficiency are not because of changes in the separation of donor and acceptor.

a) Comparison of different F/P ratio variants of antibodies

The F/P ratio of antibodies used was determined by spectrophotometry (see also in Materials and Methods). To verify the labeling ratios, cells were labeled with different F/P ratio versions of the same antibody and the mean intensities of the cells were measured. The mean intensity of cells increased with an increase in antibody F/P ratio, however the increase was not linearly proportional, with a drop off of the intensity signal especially towards the upper limit of the used F/P range (Figure 4A). The intensity curve plotted as a function of antibody F/P ratio was similar for trastuzumab and pertuzumab conjugated with the same dye (Figure 4B), whereas different dye variants of the same antibody yielded dissimilar curves. Intensity saturation was therefore dye dependent, with a loss of signal even appreciable at F/P ratios as low as 2 (in the case of Alexa Fluor 546) and increasing with an increase in antibody F/P ratio. Intensity saturation curves as a function of labeling antibody concentration were the same for different F/P ratio

variants of the same antibody (Figure 4C), indicating that antibody affinity for and binding to the recognized epitope are not altered by F/P ratios.

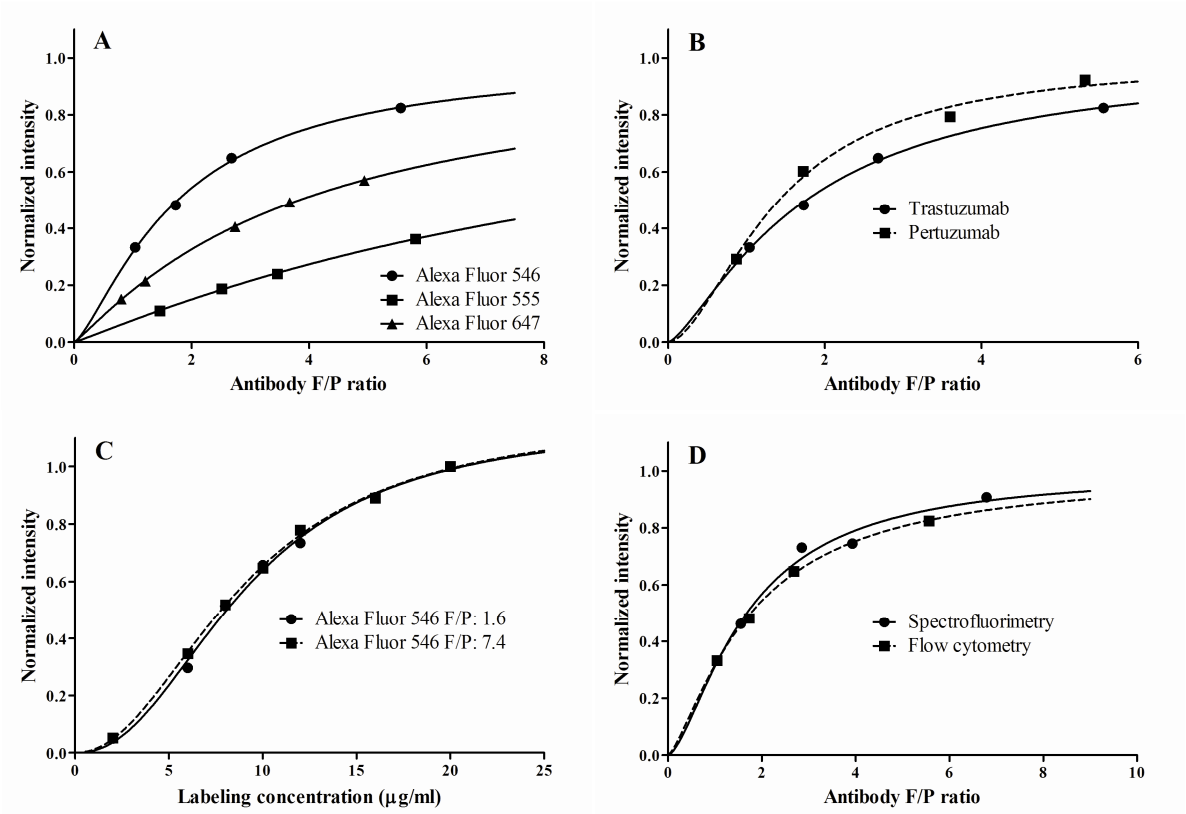

Figure 4. Dependence of fluorescence intensity on antibody labeling ratio. A) Intensity saturation as a function of antibody labeling ratio for NCI-N87 cells labeled with different fluorophores conjugated to trastuzumab. B) Intensity saturation as a function of antibody labeling ratio for NCI-N87 cells labeled with Alexa Fluor 546 conjugated with trastuzumab or pertuzumab. C) Intensity saturation as a function of antibody labeling concentration for NCI-N87 cells labeled with different F/P ratio variants of Alexa Fluor 546 conjugated trastuzumab. D) Intensity saturation as a function of antibody labeling ratio for Alexa Fluor 546 conjugated trastuzumab as measured in solution by spectrofluorimetry or for labeled NCI-N87 cells by flow cytometry.

To investigate whether binding to the cell surface can influence the optical properties of the fluorophore conjugated antibodies, flow cytometric measurements were complimented with spectrofluorimetric studies. The emission and excitation spectra of fluorophore conjugated antibody solutions were recorded to rule out the possibility of a spectral shift from increasing F/P ratio. The recorded curves did not show a shift in either the excitation or emission spectra (Figure 5). Absorption spectra were also not altered by changes in antibody F/P ratio. After correcting for concentration differences of the antibody solutions (different dilutions were used

to keep solution absorbance below 0.05 to minimize inner filter effects) intensity saturation was still evident and showed differences between the different fluorophores. The saturation of intensity as a function of antibody F/P seen with the spectrofluorimeter for free antibodies in solution was very similar to the intensity curve of the same antibody bound to the cell surface (Figure 4D). We concluded that binding to the cell surface did not influence spectral behavior of the dyes and that intensity quenching happens in a dye-specific manner between the fluorophores bound to the same antibody.

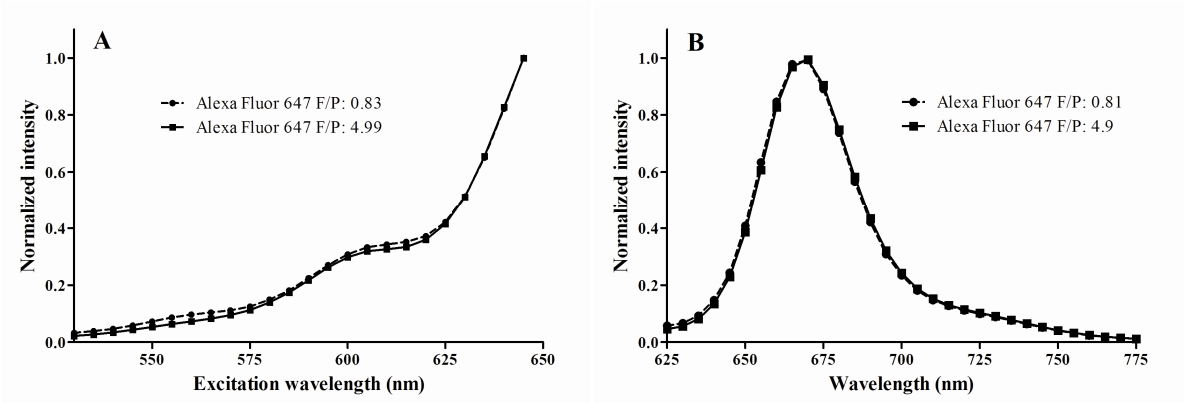

Figure 5. Measured excitation (A) and emission (B) spectra for different F/P ratio variants of Alexa Fluor 647conjugated pertuzumab.

The interaction of fluorophores bound to the same antibody was further investigated with fluorescence anisotropy measurements. Anisotropy showed linear dependence from labeled antibody concentration similar to concentration depolarization of free dyes (101); therefore anisotropy was measured at several concentrations and then plotted as a function of concentration, as opposed to comparing single measurement points (Figure 6A). The individual measurement points of antibodies were fit with a line and the y-intercept, designated by us as intrinsic anisotropy (which corresponds to the anisotropy of an infinitely dilute antibody solution and is equal to the anisotropy of a single antibody without the perturbing concentration effects), was used to compare the antibodies. We found that as the F/P ratio increased, intrinsic anisotropy decreased (Figure 6B). This change of anisotropy as a function of F/P ratio was true for all used antibodies; however the curves were characteristic for the fluorophores investigated. The anisotropy of antibody conjugated dyes was substantially higher than the anisotropy of the free dye.

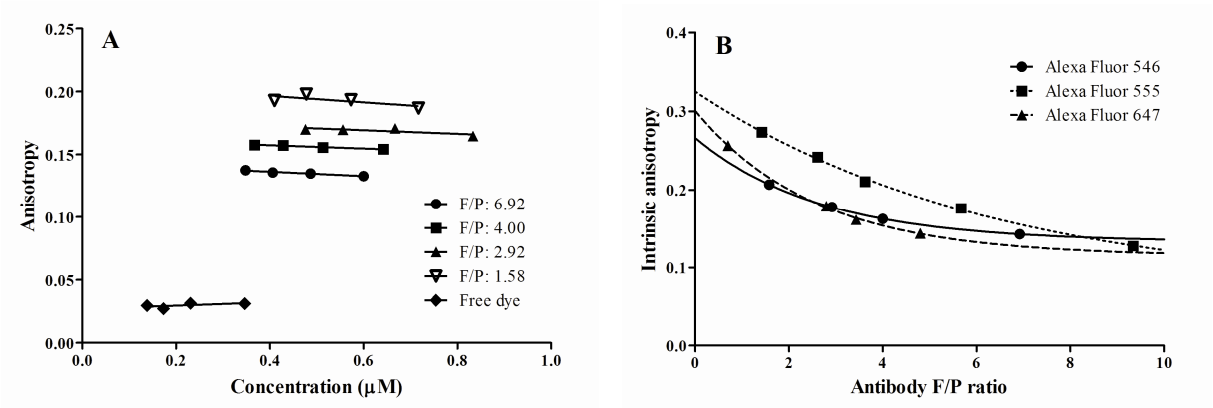

Figure 6. Anisotropy of antibody conjugated dyes in solution. A) Anisotropy of different F/P ratio variants of trastuzumab conjugated with Alexa Fluor 546 and of the free dye as a function of concentration. B) Intrinsic anisotropy as a function of antibody F/P ratio for trastuzumab conjugated with Alexa Fluor 546, Alexa Fluor 555 or Alexa Fluor 647.

b) Energy transfer measurements with different F/P ratio antibody variants

The straight forward relationship between distance, rate of transfer and measured FRET efficiency is valid only for the interaction of one donor with one acceptor. When multiple fluorophores interact, the average rate of transfer for the system can change even without any underlying distance changes (75). Increasing the number of acceptors interacting with a given donor increases the probability of an excited donor to find an acceptor partner before de-excitation and leads to an increase in the rate of transfer and subsequently in transfer efficiency. If all *n* acceptors interacting with the donor are identical in terms of FRET interaction probability, then the system's rate of transfer will be *n* times the rate of transfer for one acceptor (102,103). In this case the relationship between E_0 (the original energy transfer efficiency with one acceptor) and E_n (transfer efficiency after *n*-fold increase of the rate of transfer) is the following (see also Figure 7A):

$$E_n = \frac{n \cdot k_{transfer}}{n \cdot k_{transfer} + k_{other}} = \frac{n \cdot k_{transfer}}{k_{transfer} + k_{other}} \Bigg/ \frac{k_{transfer} + k_{other} + (n-1) \cdot k_{transfer}}{k_{transfer} + k_{other}} = \frac{nE_0}{1 + (n-1)E_0} \quad (24)$$

The seemingly complicated term can be linearized if the term $A = E/(1 - E)$ is used instead of E:

$$A_0 = \frac{E_0}{1 - E_0} \quad (25)$$

$$A_n = \frac{E_n}{1-E_n} = n \cdot \frac{E_0}{1-E_0} = n \cdot A_0 \qquad (26)$$

Therefore plotting A as a function of n yields a straight line, with A_0 as the y-intercept (Figure 7B). The value of E_0 can in turn be calculated from A_0. Since E_0 is the characteristic transfer efficiency for the interaction of one donor with one acceptor, it can be used for distance calculations according to the original Förster equations.

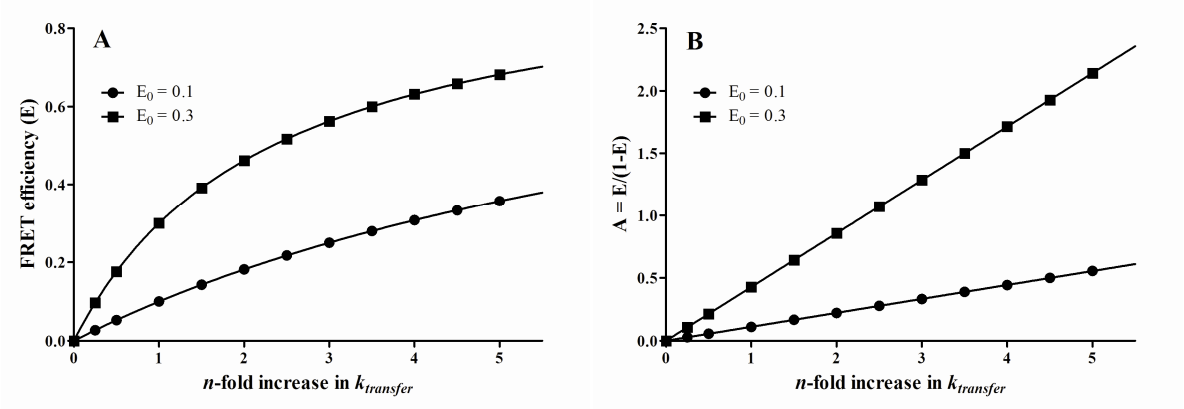

Figure 7. Effect of changes in the rate constant on energy transfer efficiency. A) Energy transfer efficiency as a function of the rate constant. B) The same data were plotted as $A = E/(1-E)$ as a function of rate constant. During the simulation only $k_{transfer}$ was changed, all other deexcitation processes remained unchanged. E_0: initial transfer efficiency measured with arbitrary initial rate of transfer.

To verify this relationship, transfer efficiency was measured between trastuzumab and pertuzumab conjugated with Alexa Fluor 546, Alexa Fluor 555 or Alexa Fluor 647. Different F/P ratio variants were used to produce changes in interacting fluorophore numbers. As discussed in the Materials and Methods chapter, the intensity-based method that we used requires determination of the alpha factor that scales for the differences of detection sensitivity of emitted donor and acceptor fluorescence. This requires that the fluorescent signal of the same number of excited donors and acceptors be compared, therefore the labeling ratios of the antibodies have to be taken into consideration (since with the same amount of bound antibodies, a higher F/P ratio will result in more fluorophores and thus higher absolute intensities without increasing detection sensitivity). The alpha factor is an instrument dependent factor; however the intensity saturation results in different alpha factors for the labeled antibodies even without changing instrument

setup (if intensities are corrected with nominal labeling ratios, since these do not reflect the actual increases in intensity). With this in mind, alpha factors were calculated with the smallest F/P ratio antibodies, which correspond to the F/P ratio range of the saturation curves where intensity can be approximated to change linearly with an increase in F/P ratio.

Cell surface FRET measurements were carried out with the donor (Alexa Fluor 546 or Alexa Fluor 555) conjugated to trastuzumab and the acceptor (Alexa Fluor 647) conjugated to pertuzumab and also with donor conjugated pertuzumab and acceptor conjugated trastuzumab. Measurements in both directions yielded similar transfer efficiency values and trends, so for simplicity we only discuss results obtained with donor conjugated pertuzumab and acceptor conjugated trastuzumab. Transfer efficiency for a given donor increased non-linearly with the increase of acceptor F/P ratio and followed the FRET saturation curve predicted by our theoretical calculations (Figure 8A and 8B). All donors had similar saturation curves, however with a shift of the curve towards higher transfer efficiency values with the increase of donor labeling ratios in the case of Alexa Fluor 546. The correlation between the labeling ratio of the donor and transfer efficiency was weak, with a calculated Pearson's correlation coefficient of 0.14 for Alexa Fluor 546 and 0.038 for Alexa Fluor 555. The measured transfer efficiency achieved with a given acceptor showed only slight increase from increasing the donor F/P ratio. On the other hand transfer efficiency was strongly correlated with the labeling ratio of the acceptor, with a Pearson's correlation coefficient of 0.95 calculated for all acceptor-donor combinations. Increasing acceptor F/P ratio drastically increased transfer efficiency with any given donor. Energy transfer also showed correlation with the acceptor-to-donor (A/D) ratio. This is however a byproduct from calculating A/D ratio as F/P ratio of the acceptor divided by F/P ratio of the donor. The non-causal relationship between A/D ratio and transfer efficiency is supported by the results showing that the same A/D ratio can result in very different transfer efficiency values depending on the individual F/P of the acceptor and very similar transfer efficiencies can be measured with different A/D ratios if the F/P ratio of the acceptor is the same (Figure 8E). The term A plotted as a function of acceptor F/P ratio showed a linear relationship as predicted by our theoretical model (Figure 8C and 8D). The slope of the fitted lines was used to determine A_0 and then calculate characteristic transfer efficiency for the dyes. The characteristic FRET efficiency was then plotted as a function of donor F/P ratio (Figure 8F) and we saw a dye-specific linear increase with an increase in donor F/P ratio.

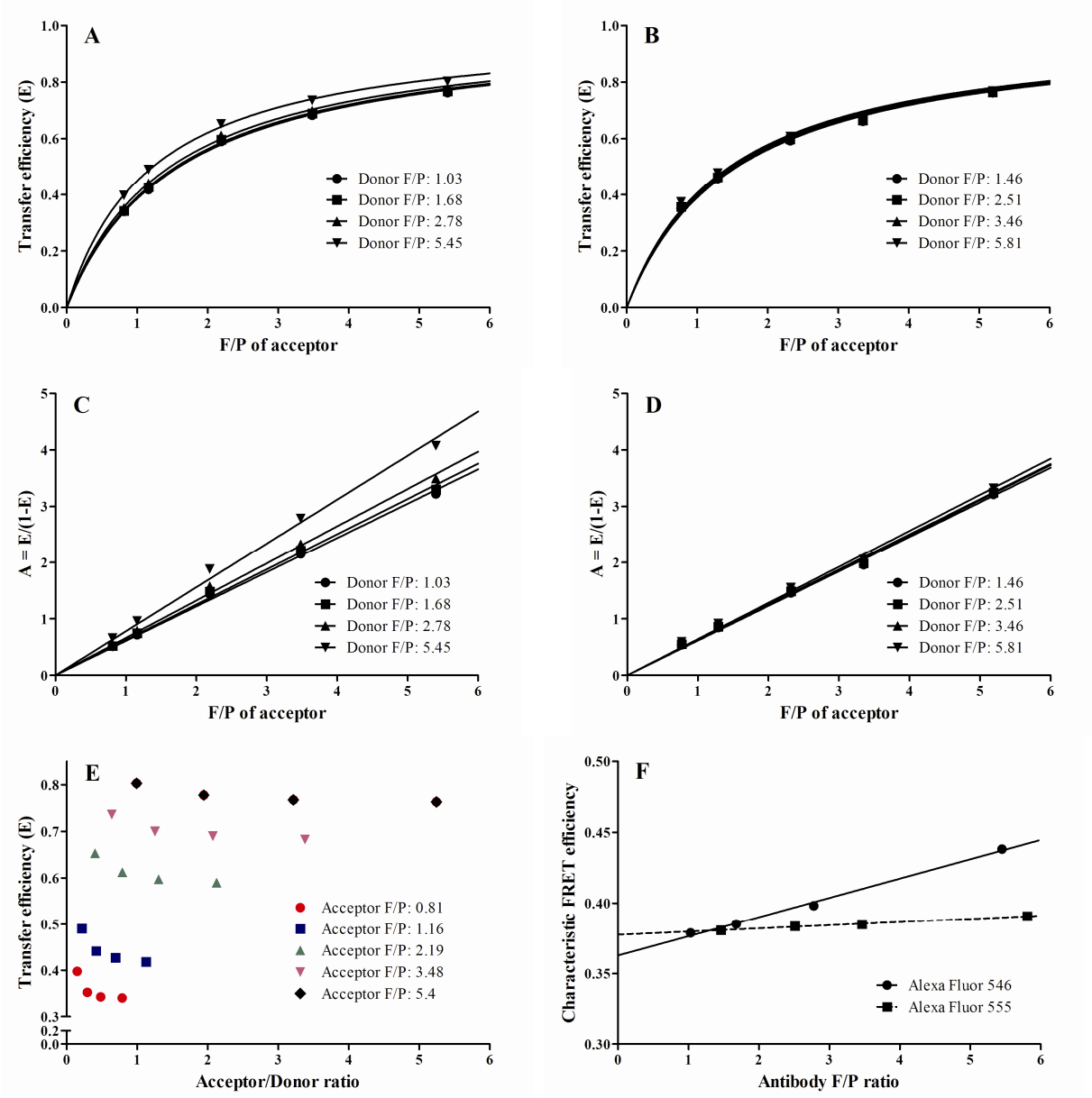

Figure 8. Dependence of FRET efficiency on antibody labeling ratio. A) and B) FRET efficiency was measured between Alexa Fluor 546 A) or Alexa Fluor 555 B) conjugated pertuzumab (serving as donors) and Alexa 647 conjugated trastuzumab (serving as acceptor) and plotted against the labeling ratio of the acceptor. C) and D) The same data were plotted as $A = E/(1-E)$ against the acceptor labeling ratio. E) Transfer efficiency as a function of acceptor/donor ratio for energy transfer between Alexa Fluor 546 conjugated pertuzumab and Alexa Fluor 647 conjugated trastuzumab. F) The characteristic transfer efficiency was plotted as a function of donor labeling ratio for Alexa Fluor 546 and Alexa Fluor 555 fluorophores. Characteristic transfer efficiency: FRET efficiency measured with acceptor labeling ratio of 1.

2. TripleFRET: a method to measure transfer efficiency in three-dye systems

a) TripleFRET calculations

Traditional FRET measurements in flow cytometry relying on donor quenching require two separate samples to determine FRET: a transfer sample labeled with both donor and acceptor and a donor only sample to determine unquenched donor intensity. Any change in labeled donor numbers (from altered expression levels, competition between labeling antibodies, etc.) leads to measurement error. This problem can be circumvented by using an intensity-based method that calculates FRET from quenched donor, sensitized acceptor and acceptor emission (see also the Literature overview). The difficulty of expanding the method to a three-dye system lies in reliably separating and identifying these emissions for all three dyes.

An initial equation set to calculate both direct and relay-transfer from dye A to C is presented below. The calculations require detection of six independent emission intensities, I_1-I_6 (see Materials and Methods for laser excitation wavelengths and emission filters). The six intensities can be interpreted as follows: I_1 – quenched emission of donor A (by acceptors B and C), native intensity channel to detect dye A; I_2 – sensitized emission (from donor A) and quenched emission of acceptor B (by acceptor C), I_3 – sensitized emission of acceptor C (from donor A and donor B excited through donor A), I_4 – quenched emission of donor B (by acceptor C), native intensity channel to detect dye B; I_5 – sensitized emission of acceptor C (from donor B) and I_6 – native intensity channel to detect dye C.

$$
\begin{aligned}
&I_1(488nm \rightarrow 530/30BP) = I_A(1-E'_{AB}-E'_{AC}) \\
&I_2(488nm \rightarrow 585/42BP) = S_1 I_A(1-E'_{AB}-E'_{AC}) + \alpha_{AB} I_A E'_{AB}(1-E_{BC}) + S_4 I_B(1-E_{BC}) \\
&I_3(488nm \rightarrow 675/20BP) = \alpha_{AC} I_A(E_{relay}+E'_{AC}) + S_{12}\alpha_{AB} I_A E'_{AB}(1-E_{BC}) + S_9 I_A(1-E'_{AB}-E'_{AC}) \\
&+S_{10} I_B(1-E_{BC}) + S_7 I_C \qquad (27) \\
&I_4(532nm \rightarrow 585/42BP) = I_B(1-E_{BC}) \\
&I_5(532nm \rightarrow 650LP) = S_2 I_B(1-E_{BC}) + \alpha_{BC} I_B E_{BC} + S_3 I_C \\
&I_6(633nm \rightarrow 650LP) = I_C
\end{aligned}
$$

The equation set assumes competitive FRET efficiencies E'_{AB} and E'_{AC} for FRET from A to B and from A to C, respectively. There are altogether seven unknowns: three unperturbed intensities I_A, I_B and I_C from the three dyes (that would be measured in the absence of FRET) and

four transfer efficiencies E'_{AB}, E'_{AC}, E_{BC} and E_{relay}. Since in its present form the equation system is underdetermined (with only six independent equations for seven variables), a further equation is required for a solution. Therefore equation (18) is used (in a slightly modified form to account for competition between dyes B and C, see also equation (22)) for a seventh independent equation:

$$E_{relay} = E'_{AB} \cdot E_{BC} \tag{28}$$

The spillover and cross-excitation factors ($S_1 - S_{12}$) are calculated from single-labeled samples in the following way (where I_p^q is the intensity in channel p of a sample labeled with only dye q conjugated to antibodies; values of S-factors and standard deviations are summarized in Table 2):

$$\begin{array}{lll} & S_2 = \dfrac{I_5^B}{I_4^B} & \\ S_1 = \dfrac{I_2^A}{I_1^A} & S_4 = \dfrac{I_2^B}{I_4^B} & S_3 = \dfrac{I_5^C}{I_6^C} \\ & & S_5 = \dfrac{I_4^C}{I_5^C} \\ S_9 = \dfrac{I_3^A}{I_1^A} & S_{10} = \dfrac{I_3^B}{I_4^B} & \\ & & S_7 = \dfrac{I_3^C}{I_6^C} \\ & S_{12} = \dfrac{I_3^B}{I_2^B} & \end{array} \tag{29}$$

Table 2
Values of S-factors and standard deviations (SD)

Factor	Value	SD
S_1	0.1588	0.00361
S_2	0.0420	0.00311
S_3	0.0574	0.00525
S_4	0.0748	0.01427
S_7	0.0151	0.00262
S_9	0.0279	0.00195
S_{10}	0.0205	0.00412
S_{12}	0.2734	0.02397

The alpha-factors can be determined empirically by the following formulas (where L^X is the labeling ratio of the antibody with fluorophore X and ε^X is the molar extinction coefficient of fluorophore X at the indicated wavelengths):

$$\alpha_{AB} = \frac{I_2^B}{I_1^A} \cdot \frac{L^A}{L^B} \cdot \frac{\varepsilon_{488}^A}{\varepsilon_{488}^B}$$

$$\alpha_{AC} = \frac{I_3^C}{I_1^A} \cdot \frac{L^A}{L^C} \cdot \frac{\varepsilon_{488}^A}{\varepsilon_{488}^C} \tag{30}$$

$$\alpha_{BC} = \frac{I_5^C}{I_4^B} \cdot \frac{L^B}{L^C} \cdot \frac{\varepsilon_{532}^B}{\varepsilon_{532}^C}$$

With our instrumental setup, S_5 was reproducibly 0, therefore it was omitted from further calculations (it was however measured each time to verify the validity of such a simplification). The equation set consisting of equations (27) and (28) can be solved, however yields complicated expression for most variables. These can be simplified with a set of factorization terms:

$$\begin{aligned}
I_{X1} &= I_1 \\
I_{X2} &= I_2 - S_1 I_1 - S_4 I_4 \\
I_{X3} &= I_3 - S_{12} I_2 - (S_9 - S_1 S_{12}) I_1 - S_7 I_6 - S_4 I_{X5} \\
I_{X4} &= I_4 \\
I_{X5} &= I_5 - S_2 I_4 - S_3 I_6
\end{aligned} \tag{31}$$

The terms correspond to bleed-through corrected sensitized emission (I_{X2}, I_{X3} and I_{X5}) and quenched donor (I_{X1} and I_{X4}) intensities. The solutions for the variables can be given as:

$$\begin{aligned}
I_A &= I_{X1} + \frac{I_{X2}}{\alpha_{AB}} + \frac{I_{X3}}{\alpha_{AC}} \\
I_B &= \frac{I_{X5} + \alpha_{BC} I_{X4}}{\alpha_{BC}} \\
I_C &= I_6
\end{aligned} \tag{32}$$

$$E'_{AB} = \frac{\alpha_{AB} I_{X2}}{(\alpha_{AB} I_{X3} + \alpha_{AC} I_{X2} + \alpha_{AB}\alpha_{AC} I_{X1})(1 - E_{BC})} = \frac{\alpha_{AC} I_{X2} (I_{X5} + \alpha_{BC} I_{X4})}{\alpha_{BC} I_{X4} \left[\alpha_{AC} I_{X2} + \alpha_{AB} (I_{X3} + \alpha_{AC} I_{X1})\right]}$$
$$E'_{AC} = \frac{\alpha_{AB} I_{X3} (1 - E_{BC}) - \alpha_{AC} I_{X2} E_{BC}}{(\alpha_{AB} I_{X3} + \alpha_{AC} I_{X2} + \alpha_{AB}\alpha_{AC} I_{X1})(1 - E_{BC})} = \frac{\alpha_{AB}\alpha_{BC} I_{X3} I_{X4} - \alpha_{AC} I_{X2} I_{X5}}{\alpha_{BC} I_{X4} \left[\alpha_{AC} I_{X2} + \alpha_{AB} (I_{X3} + \alpha_{AC} I_{X1})\right]} \quad (33)$$

$$E_{BC} = \frac{I_{X5}}{I_{X5} + \alpha_{BC} I_{X4}} \quad (34)$$

The non-competitive FRET efficiencies can also be calculated using equation (21):

$$E_{AB} = \frac{I_{X2} (I_{X5} + \alpha_{BC} I_{X4})}{I_{X2} (I_{X5} + \alpha_{BC} I_{X4}) + \alpha_{AB}\alpha_{BC} I_{X1} I_{X4}}$$
$$E_{AC} = \frac{\alpha_{AB}\alpha_{BC} I_{X3} I_{X4} - \alpha_{AC} I_{X2} I_{X5}}{\alpha_{AB}\alpha_{BC} I_{X4} (I_{X3} + \alpha_{AC} I_{X1}) - \alpha_{AC} I_{X2} I_{X5}} \quad (35)$$

Relay-transfer and total transfer are calculated from equation (28) and equation (22), respectively:

$$E_{relay} = \frac{\alpha_{AC} I_{X2} I_{X5}}{\alpha_{BC} I_{X4} \left[\alpha_{AC} I_{X2} + \alpha_{AB} (I_{X3} + \alpha_{AC} I_{X1})\right]} \quad (36)$$

$$E_{total} = \frac{\alpha_{AB} I_{X3}}{\alpha_{AC} I_{X2} + \alpha_{AB} (I_{X3} + \alpha_{AC} I_{X1})} = \frac{I_{X3}}{\alpha_{AC} I_A} \quad (37)$$

The initial equation set and solutions were co-developed with Horváth Gábor. Factorized terms, alpha- and *S*-factors are a contribution of Horváth Gábor.

b) Initial equation sets and solutions for the cases of restricted interaction schemes

As we shall later discuss, the initial equation set defines how ensemble sensitized emission is divided and assigned to a given fluorophore (and in end effect, the contribution from individual transfer efficiency). Therefore, if one or more energy transfer routes are not possible, the initial equation set has to be modified. Three further main cases are possible.

1. Relay-transfer without direct transfer from dye A to C.

The following initial equation set is used:

$$
\begin{aligned}
&I_1 = I_A(1-E_{AB})\\
&I_2 = S_1 I_1(1-E_{AB}) + \alpha_{AB} I_A E_{AB}(1-E_{BC}) + S_4 I_B(1-E_{BC})\\
&I_3 = S_9 I_1(1-E_{AB}) + S_{12}\alpha_{AB} I_A E_{AB}(1-E_{BC}) + \alpha_{AC} I_A E_{AB} E_{BC} + S_4 \alpha_{BC} I_B E_{BC}\\
&+S_{10} I_B(1-E_{BC}) + S_7 I_C\\
&I_4 = I_B(1-E_{BC}) + S_5 \alpha_{BC} I_B E_{BC}\\
&I_5 = S_2 I_B(1-E_{BC}) + \alpha_{BC} I_B E_{BC} + S_3 I_C\\
&I_6 = I_C
\end{aligned}
\tag{38}
$$

The factorization terms are the same for this case as when all transfer routes can take place. The solutions are as follows:

$$
\begin{aligned}
&I_A = I_{X1} + \frac{I_{X2}}{\alpha_{AB}(1-E_{BC})} = I_{X1} + \frac{I_{X2}}{\alpha_{AB}}\left(1 + \frac{I_{X5}}{\alpha_{BC} I_{X4}}\right)\\
&I_B = \frac{I_{X5} + \alpha_{BC} I_{X4}}{\alpha_{BC}}\\
&I_C = I_6
\end{aligned}
\tag{39}
$$

$$
\begin{aligned}
&E_{AB} = \frac{I_{X2}}{I_{X2} + \alpha_{AB} I_{X1}(1-E_{BC})} = \frac{I_{X2}(I_{X5} + \alpha_{BC} I_{X4})}{I_{X2}(I_{X5} + \alpha_{BC} I_{X4}) + \alpha_{AB}\alpha_{BC} I_{X1} I_{X4}}\\
&E_{BC} = \frac{I_{X5}}{I_{X5} + \alpha_{BC} I_{X4}}\\
&E_{relay} = E_{AB} \cdot E_{BC} = \frac{I_{X2} I_{X5}}{I_{X2}(I_{X5} + \alpha_{BC} I_{X4}) + \alpha_{AB}\alpha_{BC} I_{X1} I_{X4}}\\
&E_{total} = \frac{I_{X3}}{\alpha_{AC} I_A}
\end{aligned}
\tag{40}
$$

The energy transfer from dye A to B is not corrected in this case, since there is no competition from dye C.

2. Direct energy transfer from dye A to C without relay-transfer.

The initial equation set is as follows:

$$
\begin{aligned}
&I_1 = I_A(1-E'_{AB}-E'_{AC})\\
&I_2 = S_1 I_A(1-E'_{AB}-E'_{AC})+\alpha_{AB} I_A E'_{AB}+S_4 I_B(1-E_{BC})\\
&I_3 = S_9 I_A(1-E'_{AB}-E'_{AC})+S_{12}\alpha_{AB} I_A E_{AB}+\alpha_{AC} I_A E_{AC}+S_4\alpha_{BC} I_B E_{BC}\\
&+S_{10} I_B(1-E_{BC})+S_7 I_C\\
&I_4 = I_B(1-E_{BC})+S_5\alpha_{BC} I_B E_{BC}\\
&I_5 = S_2 I_B(1-E_{BC})+\alpha_{BC} I_B E_{BC}+S_3 I_C\\
&I_6 = I_C
\end{aligned}
\tag{41}
$$

Factorization terms are the same as before. The solutions are:

$$
\begin{aligned}
I_A &= I_{X1}+\frac{I_{X2}}{\alpha_{AB}}+\frac{I_{X3}}{\alpha_{AC}}\\
I_B &= \frac{I_{X5}+\alpha_{BC} I_{X4}}{\alpha_{BC}}\\
I_C &= I_6
\end{aligned}
\tag{42}
$$

$$
\begin{aligned}
E'_{AB} &= \frac{\alpha_{AC} I_{X2}}{\alpha_{AC} I_{X2}+\alpha_{AB} I_{X3}+\alpha_{AB}\alpha_{AC} I_{X1}}\\
E'_{AC} &= \frac{\alpha_{AB} I_{X3}}{\alpha_{AC} I_{X2}+\alpha_{AB} I_{X3}+\alpha_{AB}\alpha_{AC} I_{X1}}\\
E_{BC} &= \frac{I_{X5}}{I_{X5}+\alpha_{BC} I_{X4}}\\
E_{total} &= \frac{I_{X3}}{\alpha_{AC} I_A}
\end{aligned}
\tag{43}
$$

3. No direct of relay-transfer between dye A and C

The following initial equation set applies:

$$
\begin{aligned}
&I_1 = I_A(1-E_{AB})\\
&I_2 = S_1 I_A(1-E_{AB})+\alpha_{AB} I_A E_{AB}+S_4 I_B(1-E_{BC})\\
&I_3 = S_9 I_A(1-E_{AB})+S_{12}\alpha_{AB} I_A E_{AB}+S_4\alpha_{BC} I_B E_{BC}+S_{10} I_B(1-E_{BC})+S_7 I_C\\
&I_4 = I_B(1-E_{BC})+S_5\alpha_{BC} I_B E_{BC}\\
&I_5 = S_2 I_B(1-E_{BC})+\alpha_{BC} I_B E_{BC}+S_3 I_C\\
&I_6 = I_C
\end{aligned}
\tag{44}
$$

The solutions are (again, factorized terms remain unchanged):

$$I_A = I_{X1} + \frac{I_{X2}}{\alpha_{AB}}$$
$$I_B = \frac{I_{X5} + \alpha_{BC} I_{X4}}{\alpha_{BC}} \qquad (45)$$
$$I_C = I_6$$

$$E_{AB} = \frac{I_{X2}}{I_{X2} + \alpha_{AB} I_{X1}}$$
$$E_{BC} = \frac{I_{X5}}{I_{X5} + \alpha_{AC} I_{X5}} \qquad (46)$$

c) Transfer efficiencies of two- and three-dye systems

To verify our calculation method, an adequate model system had to be chosen. For energy transfer to occur there has to be overlap between the emission spectrum of the donor and the excitation spectrum of the acceptor. We chose the dyes Alexa Fluor 488 (dye A), Alexa Fluor 546 (dye B) and Alexa Fluor 647 (dye C) for our experiments, since Alexa Fluor 488-546 and Alexa Fluor 546-647 are well characterized FRET pairs and there is significant enough overlap between Alexa Fluor 488 and Alexa Fluor 647 to permit direct A to C transfer (see Figure 9 for relevant spectra of the dyes).

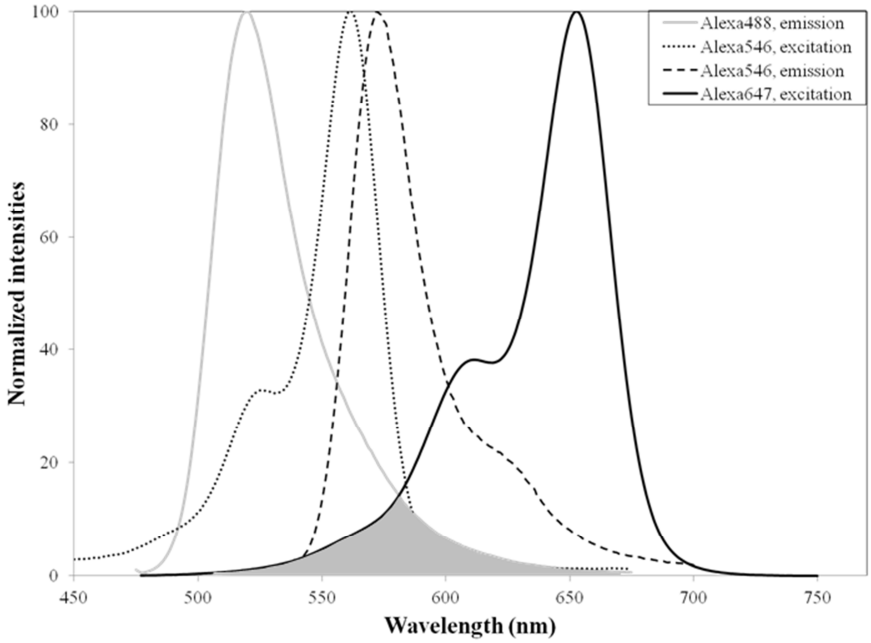

Figure 9. Normalized spectra of donor and acceptor fluorophores. The grey shaded area corresponds to the overlap integral of the emission spectrum of dye A and excitation spectrum of dye C.

NCI-N87 cells were labeled with trastuzumab, pertuzumab and H76.5 antibodies against the ErbB2 protein. These antibodies were previously shown to non-competitively bind to different epitopes within FRET interaction distance. Samples were prepared as a three-dye system as well as a corresponding set of two-dye systems (Table 3).

Table 3
Measured transfer efficiencies (%) in various dye systems

Labeling scheme	**Dye A Alexa Fluor 488**	**Dye B Alexa Fluor 546**	**Dye C Alexa Fluor 647**
Double (AB)	H76.5	trastuzumab	—
Double (AC)	H76.5	—	pertuzumab
Double (BC)	—	trastuzumab	pertuzumab
Triple	H76.5	trastuzumab	pertuzumab

	E_{AB}		E_{AC}		E_{BC}	
	Double (AB)	**Triple**	**Double (AC)**	**Triple**	**Double (BC)**	**Triple**
E as two-dye	13.5	7.9	4.9	11.4	45.1	44.3
E'	13.5	12.9	4.9	4.0	45.1	44.4
E	13.4	13.4	4.9	4.6	N.A.	N.A.

	Double	**Triple**
$\mathbf{E_{relay}}$	N.A.	5.7
$\mathbf{E_{total}}$	4.9	10.4

Measured E_{AB}, E_{AC} and E_{BC} are median transfer efficiencies in three-dye and corresponding two-dye systems. E as two-dye: traditional intensity-based FRET analysis used for two-dye systems; *E'*, *E*, E_{relay}, and E_{total} are competitive, non-competitive, relay and total FRET efficiencies calculated with the tripleFRET method; N.A.: not applicable. Standard deviations for the table entries are summarized in Table 7.

For validation purposes and to demonstrate the applicability of our method in three-dye systems, all samples were evaluated (in addition to our own equations) using the intensity-based method for two dye systems described in the Materials and Methods. The use of non-competing antibodies against different epitopes of the same protein ensured intramolecular binding and proximity of the dyes. The results of these measurements are listed in Table 3. All permutations of a two-dye system with the three fluorophores resulted in measurable transfer efficiencies (E_{AB} = 13.5%, E_{AC} = 4.9%, E_{BC} = 45.1%). Analyzing FRET in two-dye systems according to the tripleFRET method produced identical transfer efficiency values as conventional two-dye

intensity-based FRET analysis. FRET analysis of the three-dye system with tripleFRET resulted in transfer efficiency values very similar to the ones obtained in two-dye systems (E'_{AB} = 12.9%, E'_{AC} = 4.0%, E_{BC} = 44.4%). Correction for competition between the two acceptors further increased the agreement with the values from two-dye systems (E_{AB} = 13.4%, E_{AC} = 4.6%). At the same time, traditional intensity-based FRET failed to reproduce the FRET values of the two-dye systems in the triple-labeled sample. Specifically, E_{AB} was underestimated (7.9% instead of 13.4%) and E_{AC} overestimated (11.4% instead of 4.9%). The addition of dye B to the labeling scheme consisting of only dyes A and C substantially increased the total energy transferred from A to C (E_{total} = 4,9% →10.4%), providing evidence for a relay transfer process in our intramolecular model system.

Table 4

Labeling schemes and energy transfer efficiency values (%) measured for individual specimens after mixing and a single data acquisition

	Alexa Fluor 488	**Alexa Fluor 546**	**Alexa Fluor 647**
Specimen 1	pertuzumab	trastuzumab	—
Specimen 2	H76.5	trastuzumab	—
Specimen 3	H76.5	—	pertuzumab
Specimen 4	trastuzumab	—	pertuzumab
Specimen 5	trastuzumab	H76.5	pertuzumab
Specimen 6	pertuzumab	trastuzumab	H76.5
Specimen 7	H76.5	trastuzumab	pertuzumab

FRET efficiency	**AB**	**AC**	**BC**	**Relay**	**Total**
Specimen 1	**24.2**	0.0	0.0	0.0	0.0
Specimen 2	**12.3**	0.0	1.4	0.1	0.3
Specimen 3	-0.3	**4.9**	0.0	0.0	**4.8**
Specimen 4	0.0	**9.9**	0.0	0.6	**9.9**
Specimen 5	**9.8**	**9.6**	**33.0**	**2.9**	**12.4**
Specimen 6	**21.2**	**2.8**	**30.5**	**6.6**	**10.4**
Specimen 7	**13.5**	**4.5**	**44.2**	**5.5**	**10.2**

Standard deviations for table entries are summarized in Table 8.

To demonstrate the sensitivity of tripleFRET calculations and its power to dissect populations with different protein association patterns in biological systems, we mixed together the samples described in Table 4 in the same tube. Then energy transfer was measured by flow cytometry for the mixed sample. A representative dot plot and transfer efficiency histograms are shown in Figure 10.

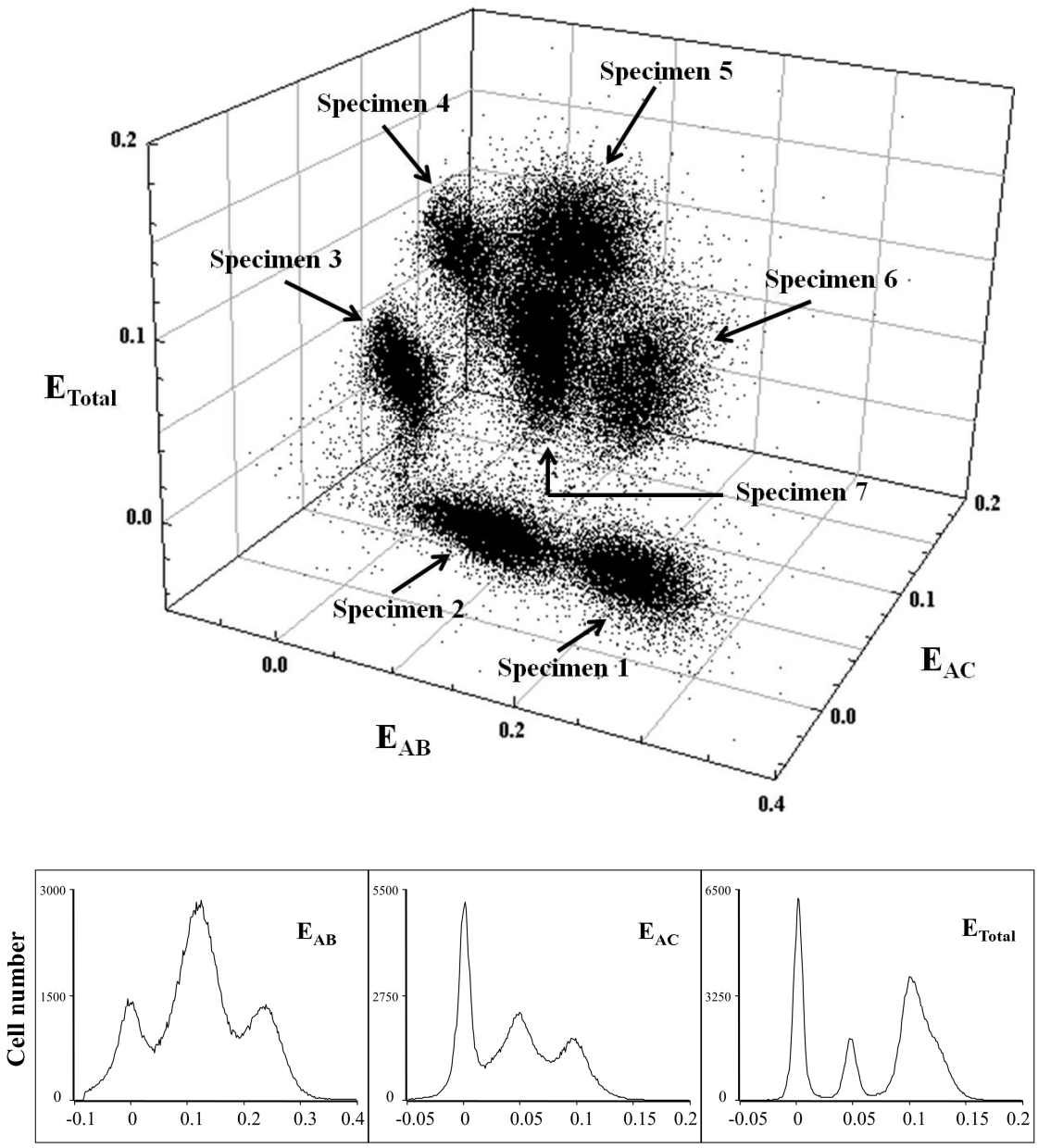

Figure 10. Three dimensional dot plot and histograms of energy transfer values determined from a mixture of seven doubly or triply labeled specimens after a single data acquisition step. The labeling schemes of the individual specimens can be found in Table 4.

As can be seen on the transfer efficiency histograms, a single measurement of transfer efficiency allows discrimination of 3 distinct populations. When only E_{AB} is measured, Specimens 1 and 6, Specimens 3 and 4, as well as Specimens 2, 5 and 7 cannot be separated from one another. When only E_{AC} is analyzed, Specimens 1 and 2, Specimens 4 and 5 as well as Specimens 3, 6 and 7 show near identical transfer efficiency distributions. Total FRET efficiency is similar in Specimens 1 and 2 as well as in Specimens 4, 5, 6 and 7. The simultaneous calculation of several transfer efficiencies is needed for discrimination of specimens that show similar transfer efficiency distributions when only one FRET value is measured. The evaluation of all 3 FRET efficiencies allowed us to discriminate between seven differently labeled specimens in the same sample. The calculated transfer efficiency values for the identified specimens are displayed in Table 3. The transfer efficiency values measured in such a fashion were in good agreement with FRET efficiencies obtained from the specimens measured individually (data not shown).

d) Sensitivity of tripleFRET measurements to changes in factor values

The robustness of a given technique depends on how reproducible and reliable the obtained values are. Two factors contribute to measurement error: random noise that arises from biological variability and instrument detection error (which lead to widening of the distribution of the measured entity) and systematic errors of measurements (which lead to shifts of distribution medians without influencing distribution width). Errors of the *S*-factors are introduced through errors in measuring intensities (which lead to random errors), therefore we consider the standard deviations to be good estimates for the errors of *S*-factors. These are summarized in Table 2. Errors of *S*- and alpha-factors will lead to systematic error of transfer efficiency values, which results in a shift of the absolute positions of populations, but preserves the relative separation between them. We compiled error propagation equations, however these are exceedingly complex and are cumbersome to interpret. Therefore we calculated the shifts in transfer efficiency from a hypothetical, 10% increase of each factor (Table 5).

Table 5

Sensitivity of measured transfer efficiencies to changes in factor values.

Sample 1	**AB**	**AC**	**BC**	**Total**
S_1	**-20.75%**	**33.91%**	-0.01%	0.82%
S_2	-0.54%	**1.72%**	-0.69%	0.10%
S_3	**-2.12%**	**6.88%**	**-2.72%**	0.19%
S_4	**-9.22%**	**13.51%**	0.00%	-0.29%
S_7	0.08%	**-1.97%**	0.00%	-0.71%
S_9	0.04%	**-1.35%**	0.00%	-0.48%
S_{12}	0.08%	**-1.97%**	0.00%	-0.67%
α_{AB}	**-8.51%**	**12.92%**	0.00%	0.00%
α_{AC}	0.90%	**-20.88%**	0.00%	**-8.19%**
α_{BC}	**-3.94%**	**12.16%**	**-5.27%**	0.03%

Sample 2	**AB**	**AC**	**BC**	**Total**
S_1	**-7.47%**	**23.13%**	0.00%	0.75%
S_2	-0.69%	**5.61%**	**-1.83%**	**-3.27%**
S_3	**-3.36%**	**26.31%**	**-8.71%**	0.24%
S_4	**-4.67%**	**12.43%**	0.00%	-0.19%
S_7	0.13%	**-4.17%**	0.00%	**-1.18%**
S_9	0.05%	**-1.66%**	0.00%	-0.47%
S_{12}	0.14%	**-4.66%**	0.00%	**-1.32%**
α_{AB}	**-7.70%**	**21.57%**	0.00%	0.00%
α_{AC}	0.84%	**-28.39%**	0.00%	**-8.18%**
α_{BC}	**-2.60%**	**19.84%**	**-6.72%**	0.00%

Sample 3	**AB**	**AC**	**BC**	**Total**
S_1	**-21.42%**	**10.73%**	0.00%	**2.19%**
S_2	-0.69%	0.82%	**-1.47%**	0.04%
S_3	**-2.59%**	**3.18%**	**-5.77%**	0.13%
S_4	**-10.36%**	**4.61%**	0.00%	0.61%
S_7	0.09%	-0.93%	0.00%	-0.63%
S_9	0.05%	-0.57%	0.00%	-0.39%
S_{12}	0.08%	-0.86%	0.00%	-0.60%
α_{AB}	**-8.53%**	**3.90%**	0.00%	0.63%
α_{AC}	**1.07%**	**-11.44%**	0.00%	**-8.11%**
α_{BC}	**-2.84%**	**3.28%**	**-6.42%**	0.00%

Table 5 continued

Transfer efficiency	AB	AC	BC	Total
Sample 1	12.8	4.1	44.3	10.4
Sample 2	22.6	2.8	28	10.8
Sample 3	9.9	8.6	31.4	11.8

Shown are the relative changes of transfer efficiencies after a 10% increase in the indicated factor value. The AB and AC transfer values are not corrected for competition. The labeling schemes for the different samples are as follows (in the order of antibody tagged with Alexa Fluor 488 – 546 – 647): Sample 1: H76.5 – trastuzumab – pertuzumab; Sample 2: pertuzumab – trastuzumab – H76.5; Sample 3: trastuzumab – H76.5 – pertuzumab. The absolute transfer efficiency values are given in percentage (%).

From the table it is easy to see, that each factor has a different influence on transfer efficiency and that the effect of a given factor strongly depends on the measured intensities and their ratio to one another (which of course are influenced by the actual real transfer efficiencies). The relative changes in Table 5 correspond to maximal changes of 2-3% in the absolute value of transfer efficiency. This is for the factors with the greatest influence on FRET and in the exaggerated case of 10% error. Based on the standard deviations of the *S*-factors, we would expect smaller real shifts. Table 7 allows us to compare standard deviations of transfer efficiency distributions calculated with either two-dye FRET or tripleFRET. In two-dye systems, tripleFRET suffers from wider population distributions, which is due to the contribution of background noise from native intensity channels of the fluorophore missing from the labeling scheme (AC transfer is affected the most). In three-dye systems, this effect no longer applies, bringing FRET distribution width closer to that seen with two-dye FRET.

Regarding the reproducibility and significance of measured differences of transfer efficiencies, we have found the standard deviation for averages of transfer efficiency means from independent experiments to be between 2 and 4.5%. This translates into a CV of 5-10% depending on the absolute value of energy transfer. Therefore we would consider FRET changes exceeding 2-5 absolute percent (depending on the measured transfer efficiency) between experiments and samples to be significant and not just introduced by measurement error. Within the same measurement setup, probably even a lower margin is acceptable. This of course is only for one type of transfer efficiency; if more are viewed simultaneously, sample discrimination should improve.

e) TripleFRET in three-dye systems with different spatial distributions of dyes

Lastly, we altered the labeling scheme (see Figure 11) so that the three dyes could not co-localize on the same protein due to competition between antibodies. This way we either achieved a dye configuration where the transfer process from A to B is intermolecular (Sample 2) or dye B excited by energy transfer from dye A was not in close proximity of dye C (Sample 3), causing relay-FRET to become minimal (Figure 11).

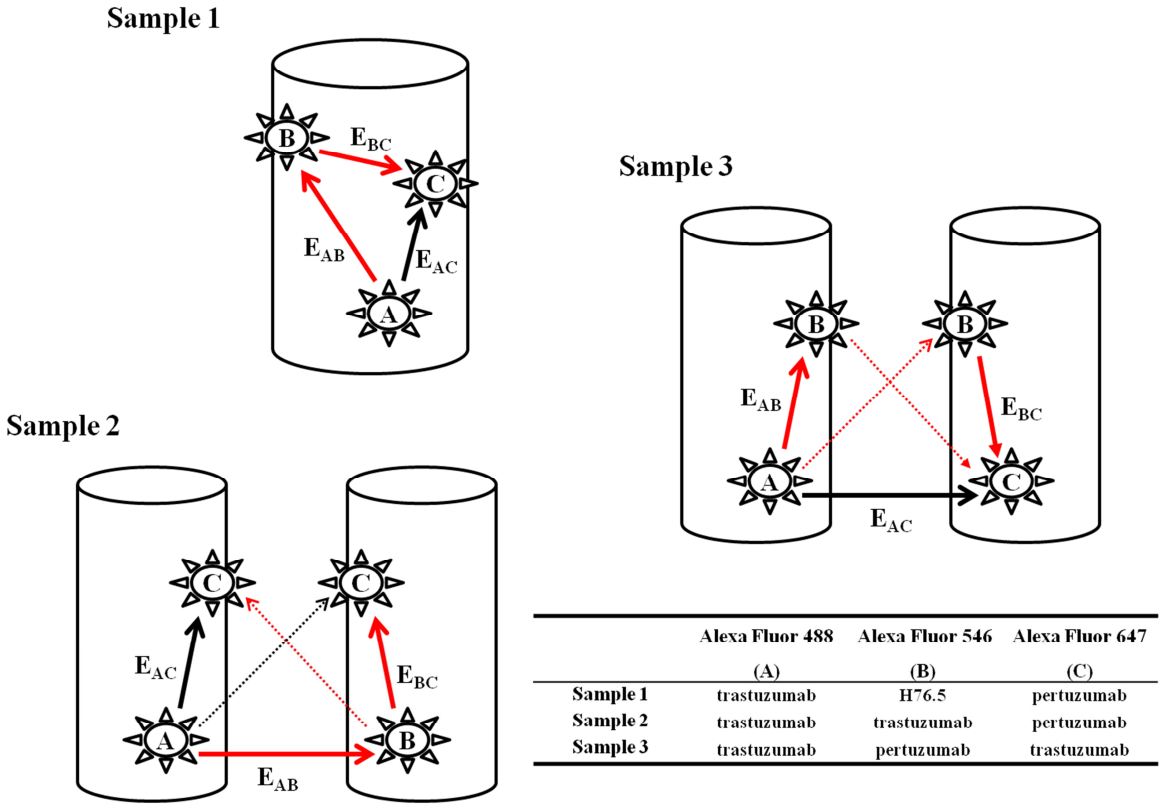

	Alexa Fluor 488 (A)	Alexa Fluor 546 (B)	Alexa Fluor 647 (C)
Sample 1	trastuzumab	H76.5	pertuzumab
Sample 2	trastuzumab	trastuzumab	pertuzumab
Sample 3	trastuzumab	pertuzumab	trastuzumab

Figure 11. Labeling schemes employed to provide alternative spatial distribution and possible transfer routes between fluorescently tagged antibodies. Bold arrows: primary transfer routes, dashed arrows: secondary transfer routes, red arrows: transfer routes potentially involved in relay-FRET.

Transfer efficiency was calculated with different initial equation sets considering four scenarios: simultaneous relay and direct transfer from A to C; only relay transfer without direct transfer; only direct transfer without relay transfer; no relay or direct transfer. Results and comparison with two-dye, dominantly intramolecular FRET values are summarized in Table 6.

Table 6

Comparison of measured transfer efficiencies (%) calculated with different initial equation sets for labeling schemes described in Figure 11

Sample 1	AB	AC	BC	Relay	Total
Relay and direct FRET	10.8 (9.9)	9.6 (8.6)	31.4	3.0	11.8
Only relay-FRET	10.8	–	31.5	3.3	12.6
Only direct FRET	7.7 (6.8)	12.6 (11.7)	31.5	–	11.7
No relay or direct FRET	7.7	–	31.5	–	13.3
In two-dye system	10.8	10.2	25.0	–	10.2

Sample 2	AB	AC	BC	Relay	Total
Relay and direct FRET	2.7 (2.4)	11.2 (10.9)	43.8	1.0	12.2
Only relay-FRET	2.7	–	43.8	1.1	13.5
Only direct FRET	1.5 (1.3)	12.1 (12.0)	43.8	–	12.0
No relay or direct FRET	1.5	–	43.8	–	13.6
In two-dye system	3.6	10.2	45.1	–	10.2

Sample 3	AB	AC	BC	Relay	Total
Relay and direct FRET	22.7 (23.6)	-2.8 (-2.2)	22.4	5.0	3.4
Only relay-FRET	22.6	–	22.4	5.0	2.8
Only direct FRET	18.3 (17.8)	3.4 (2.8)	22.4	–	2.8
No relay or direct FRET	18.5	–	22.4	–	3.5
In two-dye system	20.4	2.2	41.0	–	2.2

The displayed E_{AB} and E_{AC} values are non-competitive FRET values. Competitive FRET values are given in parenthesis where applicable. Standard deviations for table entries are summarized in Table 8.

In the case of Sample 1, the scheme supposing direct and relay transfer to dye C gave the best approximation of energy transfer values from two-dye systems without neglecting any transfer processes. The same was true for Sample 2, where assuming only relay transfer neglected the substantial direct transfer process from dye A to C and supposing only direct-FRET underestimated energy transfer from A to B. However, for Sample 3, analysis involving simultaneous direct and relay transfer failed to give results with a physical meaning, as A to C transfer was found to be negative. Calculations with only relay transfer produced a relay-FRET value that was higher than the total energy transfer from A to C. Therefore a scheme involving only direct transfer gave the best results, with physically plausible results obtained for all

calculated transfer efficiencies. However, in this case a small but relevant amount of relay transfer was neglected, since total transfer was higher in the three-dye system than in a system with only dyes A and C. As we shall later discuss, in Sample 3 several different spatial distributions are measured at the same time, which causes calculations assuming a single, homogenous distribution to become inaccurate.

Table 7
Median FRET and standard deviation (SD) values for the entries in Table 3 of the main text. All values are percentage (%)

		E as two-dye		**TripleFRET**	
		E (Median)	**SD**	**E (Median)**	**SD**
Two-dye system	E_{AB}	13.47	2.735	13.45	2.791
	E_{AC}	4.85	0.624	4.88	8.271
	E_{BC}	45.13	3.788	45.12	3.832
Three-dye system	E_{AB}	7.95	2.407	13.43	3.891
	E_{AC}	11.45	1.054	4.61	2.389
	E_{BC}	44.32	4.112	44.42	3.514
	E_{relay}	–	–	5.66	1.939
	E_{total}	–	–	10.42	0.971

Table 8
Median FRET and standard deviation (SD) values for the entries in Table 4 of the main text. All values are percentage (%)

FRET efficiency	**AB**	**SD**	**AC**	**SD**	**BC**	**SD**	**Total**	**SD**
Specimen1	24.20	2.01	–	–	–	–	–	–
Specimen2	12.32	2.04	–	–	–	–	–	–
Specimen3	–	–	4.91	0.83	–	–	4.79	0.41
Specimen4	–	–	9.86	0.81	–	–	9.87	0.46
Specimen5	9.79	2.02	9.59	1.02	32.96	6.19	12.42	0.61
Specimen6	21.22	2.61	2.85	2.17	30.55	10.05	10.43	0.63
Specimen7	13.49	2.30	4.50	1.76	44.19	9.04	10.15	0.58

Table 9

Median FRET and standard deviation (SD) values for the entries in Table 6 of the main text. All values are percentage (%)

Sample1	AB	SD	AC	SD	BC	SD	Total	SD
Relay and direct FRET	10.84	3.86	9.59	1.72	31.44	4.73	12.61	1.30
Only relay-FRET	10.85	3.86	–	–	31.45	4.68	–	–
Only direct FRET	7.65	2.85	12.59	1.33	31.51	4.76	–	–
No relay or direct FRET	7.69	2.85	–	–	31.50	4.65	–	–

Sample 2	AB	SD	AC	SD	BC	SD	Total	SD
Relay and direct FRET	2.71	5.99	11.19	2.63	43.81	6.32	12.15	1.40
Only relay-FRET	2.72	5.96	–	–	43.78	6.51	–	–
Only direct FRET	1.53	3.31	12.13	1.37	43.84	6.30	–	–
No relay or direct FRET	1.53	3.40	–	–	43.84	6.24	–	–

Sample 3	AB	SD	AC	SD	BC	SD	Total	SD
Relay and direct FRET	22.65	5.27	2.84	3.03	22.40	4.13	3.45	1.17
Only relay-FRET	22.65	5.29	–	–	22.41	4.16	–	–
Only direct FRET	18.41	4.42	3.44	1.13	22.44	4.13	–	–
No relay or direct FRET	18.49	4.35	–	–	22.45	4.05	–	–

Transfer efficiency values in Tables 7-9 are median values for distribution histograms. Standard deviations are also calculated from distribution histograms.

VI. Discussion

1. Effect of multiple FRET partners interacting simultaneously

The allure of energy transfer measurements lies in gaining spatial data for intermolecular distances far below the resolution of the imaging modality applied (nm-s as opposed to 100-s of nm-s/μm-s) (5,105-107). A plethora of methods have been developed, each focusing on a different aspect of the changes in the behavior of dyes that accompany energy transfer. As all methods that detect dye emission or intensity, the reliability of the method is only as good as the reliability of the signal that is detected. Usually, a lot of effort is put into filtering out non-specific signal components (including, but not limited to: background correction, correction for bleed-through and cross-excitation, etc) (108,109) to arrive at the "true" signal of the fluorophore of interest. However, little thought is put into how these emission profiles are produced at the molecular level and are treated "as is", an intrinsic property of the dye system. This concept can be misleading, since (as previously discussed), some methods are susceptible to signal averaging and all are sensitive to molecular level influences of transfer efficiency. Of course, some factors can be assumed to be constant for a given experiment (e.g. concentration of oxygen or other soluble quenchers, index of refraction of the conveying medium) and do not influence changes in dye signals and transfer efficiency. Then again, some factors that are introduced by the method of choice can influence the measured transfer efficiency (4,17,110-112). The effect of all these factors is important, because they determine whether the take-home message of biophysics lectures - that transfer efficiency change is influenced only by intermolecular distance change - is valid for the given experiment.

In our study we set out to establish the effect of multiple fluorophores interacting simultaneously on measured transfer efficiency. This effect can be relevant for several reasons. Movement, aggregation and sequestration that accompany biological processes can lead to changes in protein signatures and alter interacting fluorophore populations (50). Also, fluorophores are added in at least a semi-controlled fashion by the scientist into the observed system. Understanding how the fluorophores influence the measured system is crucial for correct interpretation of transfer efficiency values and accurate distance measurements. Finally, knowledge of dye interactions allows better experiment planning and opens the door to manipulating dyes in a fashion that serves better detection sensitivity and dynamic range. For our experiments we used different F/P

ratio variants of antibodies. This way we ensured that multiple fluorophores were in FRET range and we could alter their numbers in a controlled fashion to demonstrate the effects of donor and acceptor abundance in a cellular cell-surface system. While we specifically demonstrate the effects of antibody F/P ratio, the conclusions for the effects of donor and acceptor abundance are generally applicable.

a) Intensity quenching and anisotropy of antibodies

First, we compared the properties of the different F/P ratio variants of the antibodies. We encountered a non-linear increase in fluorescent signal with increasing antibody F/P ratio, implying loss of signal through quenching or some other effect. We first hypothized, that antigen recognition and/or binding might be influenced by the F/P ratio. Every additional fluorophore bound to an antibody increases the overall bulk of the dye-antibody complex. This theoretically can result in restricted movement and limit the shortest distance of approach and hinder binding of the antigen by the antibody. Additionally, the dyes can obstruct the antigen recognition region of the antibody and further inhibit binding. However, labeling antibody concentration dependent intensity saturation curves were nearly identical (after normalization to maximum intensity) for small and large F/P ratio antibodies, so F/P ratio did not influence antibody binding. Free antibodies in solution displayed the same F/P ratio dependent intensity saturation as our cellular experiments, which further ruled out an influence of antibody-antigen interaction. We also investigated whether different F/P ratio variants of the same antibody differ in absorption, excitation or emission spectra. A shift in either spectrum would result in a loss of signal mimicking saturation: a shift relative to fixed bandwidth emission filters would result in an unequal intensity-clipping for different antibodies; a shift in excitation spectra would result in different excitation efficiency from a fixed wavelength excitation source. Our data did not show any significant differences in the spectra of the different F/P ratio variants, therefore this was also ruled out as a cause of intensity saturation. The F/P ratio dependent saturation curves were different for different dyes bound to the same type of antibody, whereas different antibodies conjugated with the same dye had similar curves. Therefore the saturation effect was characteristic for the dye used.

Antibody variants were further characterized with anisotropy measurements. Anisotropy quantifies the degree of polarity lost between fluorescent emission and excitation by a polarized

excitation light. A lower anisotropy value indicates a larger shift between excitation and emission polarity. The degree of shift is determined by two main factors: the time that elapses between excitation and emission (which is determined by the fluorescence lifetime) and the speed of rotation (which is characterized by the rotational time constant). To compare the anisotropy of different F/P ratio variants, we compared the intrinsic anisotropies introduced in the Results chapter (this intrinsic anisotropy of a single freely moving fluorophore conjugated antibody is not to be confused with the intrinsic anisotropy that commonly refers to the anisotropy of a fluorophore frozen in movement). As expected, the free dye had substantially lower anisotropy than the antibody conjugated variants, a consequence of slowed movement from the added bulk of the antibody. Interestingly, intrinsic anisotropy decreased with an increase in antibody F/P ratio. This cannot be explained with just the increased complex size of higher F/P ratio variants (further decrease in movement speed from the increase in size of the dye-antibody conjugate from additional dyes should actually increase anisotropy). Several processes can take place between the dyes conjugated to the same antibody that alter anisotropy. Homo-FRET is a FRET process where both donor and acceptor belong to the same dye species and is possible because of the overlap between emission and excitation spectra of any given dye (113). Homo-FRET allows excitation energy to be passed from one dye to the other without fluorescent emission. While the individual excited dye state is shortened just as with hetero-FRET, actual fluorescent emission will occur later than without homo-FRET. Also, since FRET does not require emission and excitation dipoles to be perfectly aligned, the emission polarity can be changed in leaps. The combined effect is diversification of emitted light directions by homo-FRET, which reduces anisotropy (114-116). On the other hand, collision quenching for instance shortens the fluorescence lifetime (117) and causes an increase in measured anisotropy. Our measurements show that increasing F/P ratio reduces the anisotropy, which suggests that homo-FRET is the dominant underlying process. The minimal value of intrinsic anisotropy was correlated with the F/P ratio dependent intensity quenching exhibited by an antibody, i.e., the larger the intensity saturation of an antibody, the higher the plateau value of intrinsic anisotropy. This is in line with the assumption that intensity saturation is a consequence of collision quenching, therefore larger saturation means more quenching which can counteract the effects of homo-FRET.

b) Effects of acceptor abundance

Our FRET experiments showed the labeling ratio of the acceptor to be highly correlated with the measured transfer efficiency. Transfer efficiency measured with the same donor and different F/P ratio acceptor variants increased non-linearly with the labeling ratio. The experimental measurement points closely matched the theoretical curves predicted by our calculations. The $A = E/(1-E)$ plots also displayed the linear relationship that our theory postulated. The fact that plotting $E/(1-E)$ as a function of the acceptor labeling ratio yields a line demonstrates that each acceptor dye behaves similarly, increasing the probability of FRET interaction to the same extent. Also, our transfer efficiency curves as a function of acceptor F/P ratio closely resemble previously published curves for varying concentrations of dyes randomly distributed in solution (18), further supporting our theory that acceptors bound to a single antibody have a non-preferential, equal chance to interact with the same donor. Our measurements prove acceptor availability as a limiting factor for measured FRET efficiency. Measured transfer efficiency was increased nearly two-fold just by increasing the acceptor F/P ratio.

c) Effects of donor abundance

Theoretically, increasing the number of donor dyes does not increase the probability of an individual donor to interact with an acceptor (although an individual acceptor interacts with more donor dyes) and so the fraction of donor molecules losing the absorbed energy through FRET does not change and transfer efficiency stays unchanged. Multiple donors interacting with an acceptor should not affect transfer efficiency negatively, since donor de-excitation is such a fast process, that the chance of two simultaneously excited donors competing for the same acceptor is minimal. (Competition between donors would only present a problem if the dye system could be driven into saturation with a high enough flux of exciting photons. However at such high photon flux photobleaching would be very prominent, rendering FRET measurements impractical.) Therefore under conventional circumstances systems with multiple donors within interaction distance of the same acceptor (such as antibodies labeled with multiple dyes) are regarded as a single donor system with respect to transfer probability.

In our experiments we saw a slight increase of transfer efficiency from the increase of donor F/P ratio, which was especially evident with the Alexa Fluor 546 dye as donor. The same was true for characteristic transfer efficiency, with a linear increase with increasing donor labeling ratio.

This effect is most likely caused by the increasing homo-FRET between the donor dyes upon increasing the number of dyes bound to the antibody. The effect of homo-FRET can be explained as follows (see also Figure 12). As the donor and acceptor move through their possible spatial positions, the relative orientation of the donor emission and acceptor excitation dipoles also constantly change, cycling from relative orientations favoring FRET transition to ones that essentially preclude it (59). This orientation is taken into consideration with the κ^2 parameter in the equation for R_0. The rate of transfer depends on R_0 (see equation (2)), and through it on the orientation factor. The value of κ^2 is an averaged value for all the possible orientations, but actually changes dynamically as the fluorophores rotate. From the donor's stand point this means in certain positions κ^2 is large and FRET is likely and therefore dominates other de-excitation processes, such as fluorescence. In other positions κ^2 is small and FRET transitions are not likely (small rate of transfer), therefore other de-excitation processes determine the fate of the excited state.

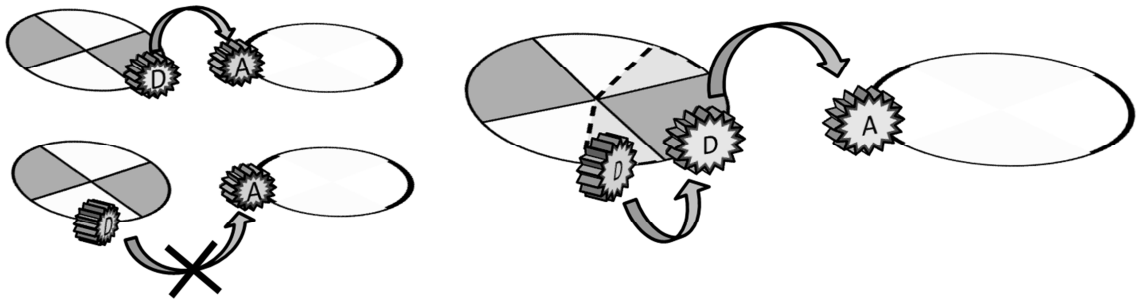

Figure 12. Possible effect of homo-FRET on measured hetero-FRET. As the donor moves through its possible spatial positions it cycles through relative dipole orientations favorable (dark grey shaded areas) and not favorable (white areas) for hetero-FRET. Homo-FRET can transfer energy from positions with low hetero-FRET probability to positions that favor hetero-FRET (light grey areas). D: donor fluorophore, A: acceptor fluorophore.

In our proposed model homo-FRET acts as a lifeline for the excited state in positions where κ^2 is small and de-excitation would take place without a contribution from FRET. Instead of non-FRET de-excitation, the donor's excited state can be conserved and transferred by homo-FRET to positions that favor FRET. One could argue that homo-FRET will also 'steal' the excited state from positions where FRET is likely. However it has been shown, that the number of possible orientations where κ^2 is maximal is fewer than the number of orientations, where κ^2 is minimal (this is also reflected in the averaged $^2/_3$ value for κ^2, which is closer to the theoretical minimum

value of 0, than to the theoretical maximum of 4) (59). It follows that homo-FRET is likelier from low κ^2 positions, since the excited donor spends more time in these positions. In short, homo-FRET by transferring energy from positions where FRET has negligible probability increases the average of κ^2, which results in a larger R_0 and larger FRET efficiency without a decrease in acceptor-donor distance.

d) Implications for FRET measurements

FRET stoichiometry measurement is a developing field that was born from the realization that most FRET measurement techniques involve the recording of apparent transfer efficiencies. This apparent FRET signal is a consequence of the inherent signal averaging in FRET measurement methods, i.e. even the smallest resolution unit (be it a cell in the flow cytometer or a pixel in a microscope image) in FRET experiments has a signal averaged from multiple fluorophores within the resolution unit. This way signals from interacting and non-interacting fluorophore populations all contribute to emission profiles of acceptors and donors. The stoichiometry methods work around this problem by utilizing a calibration standard, i.e. FRET efficiency for the used fluorophore pair is measured with a standardized construct containing one donor and one acceptor (the ratio which we also advocate as necessary for absolute distance measurements) interacting at a distance characteristic for the viewed system (this would be analogous with our term E_0). The fraction of interacting fluorophores (stoichiometry) is then calculated from the apparent FRET signal in the knowledge that actual FRET between donor and acceptor is equal to the characteristic FRET obtained with the calibration construct.

FRET stoichiometry measurements therefore have the prerequisite that despite changing interacting fractions the FRET process involves one donor and one acceptor with a constant FRET interaction and changes in apparent FRET are due to changes in the proportion of averaged signals. This criteria is met when interaction is restricted to two molecules (e.g. receptor-ligand binding). Our experiments show that when multiple interaction partners are permitted in the FRET process, a change in interacting fractions can alter the molecular level FRET (a shift from E_0 to E_n in our terminology). Under these circumstances FRET stoichiometry cannot accurately measure the total fraction of donors and acceptors participating in FRET. Also, changes in the number of acceptors interacting with donors in a given FRET process will not be unmasked. In these situations probably a lifetime-imaging approach is recommended.

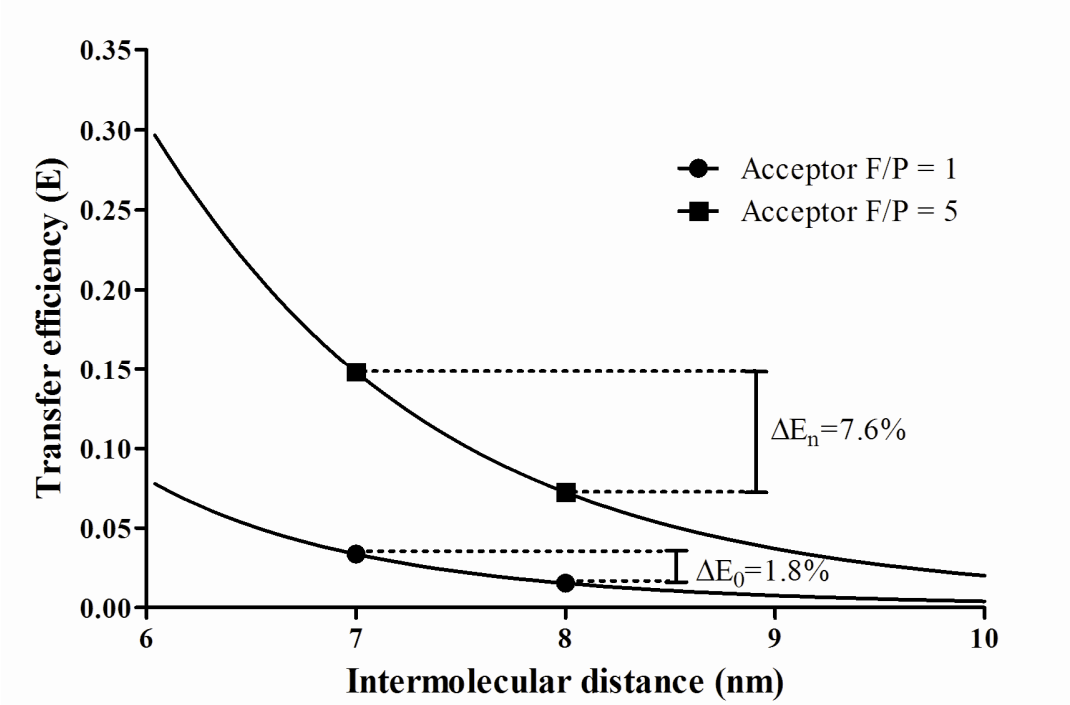

Figure 13. Simulated distance-FRET response curves. Theoretical curves showing the FRET efficiency differences for intermolecular distances of 7 and 8 nm when measured with acceptor F/P = 1 (ΔE_0) and acceptor F/P = 5 (ΔE_n) and R_0 = 4 nm.

Our results show that manipulating antibody labeling ratios can be a simple tool for increasing measurement sensitivity beyond a better signal/noise ratio of the measured intensities. Based on our results the R_0 of the acceptor-donor dye system can be manipulated by changing the labeling ratios. If we denote R_n as the Förster distance for a FRET system with n acceptors, then by substituting equation (4) into (24), the relationship between R_n and R_0 is:

$$E_n = \frac{n \cdot R_0^6}{n \cdot R_0^6 + R^6} = \frac{R_n^6}{R_n^6 + R^6} \tag{47}$$

$$R_n = n^{\frac{1}{6}} \cdot R_0 \tag{48}$$

Although this does not seem like a significant increase in R_0, it still leaves a lot of room for manipulation of the FRET system (see Figure 13). Simply by changing the R_0 of the system we can shift the intermolecular distance-FRET response curve. Therefore by increasing acceptor labeling ratio the value of FRET efficiency can be increased. This can be useful in low-FRET

systems, where FRET levels can be elevated to detectable levels above background. Further, the curve can be shifted so that all possible distance changes in a given system are followed by a significant change in FRET. For instance reducing acceptor F/P ratio can be beneficial, if FRET values are near saturation, since a smaller F/P acceptor reduces system R_0 and increases FRET change over that particular distance range. The benefit of this approach is that FRET sensitivity is increased without having to choose a new acceptor-donor pair which involves re-measuring the ratio of the molar extinction coefficients of the fluorophores at the donor excitation wavelength, recalculating R_0 and re-optimizing the measurement setup for the new dyes, if it is at all possible (e.g., availability of different excitation wavelengths in a laser is limited, available emission filters, etc.).

The concept has been recently utilized to extend the Förster-distance of protein systems, so that transfer efficiency is detectable at intermolecular distances of 15 nm (118). Labeling the protein of interest with multiple acceptors randomly distributed on the protein surface elevated transfer efficiency above the level measured when just a single acceptor is used. Although with this approach the acceptor can no longer be treated as having a well defined, point-like distance from the donor, it allows detection of protein interaction at distances exceeding the conventional range of FRET experiments. This should allow a much broader mapping of molecular networks to encompass interaction partners that were missed because of the distance restrictions that apply to energy transfer measurements.

2. TripleFRET measurements

FRET measurements have gained wide acceptance as a means of following changes in molecular distance and association. However, the fact that FRET requires a close proximity of the donor and acceptor dyes has limited the dynamic range of these measurements. Recent studies have shown that, by adding a third dye, the dynamic range of FRET can be extended via relay-FRET. With the addition of a new dye, new energy transfer pathways are opened, which may compete with the pathways already known from a two-dye system. The untangling of these pathways not only allows for a larger FRET range, but also has the potential to study the proximity relationship of three labeled molecules at the same time. Given the complexity of protein networks in signaling pathways, such an extension can be quite important in the quantitative description of protein interactions in signaling processes.

a) TripleFRET: a novel method to measure energy transfer in three-dye systems

Previous methods for measuring transfer efficiency between three fluorophores either relied on complicated fusion protein constructs (86,119-121), were developed for dyes in solution and not adaptable for flow cytometers (80,81,87-89,122), or needed a reference sample to determine the quantity of the donor dye (dye A) for proper calibration of transfer efficiencies. While the latter approach is also used and accepted as the simplest method for calculating transfer efficiency in two-dye systems (123), it carries the risk of skewed results if the quantity of the dye changes between samples. In experiments with antibodies conjugated with fluorescent dyes, the probability for this is small as long as there is no competition between the antibodies. However, when fluorescent protein coupled proteins are expressed in a cellular system, expression efficiency can vary from cell-to-cell and this effect is even more accentuated when multiple exogenous proteins are expressed (124). Therefore, we sought to develop a method which does not rely on an external reference sample to calculate transfer efficiency. We identified and broke down to quantifiable components six different emission intensities in total, which, in a system of equations allow the individual FRET between each member of the system to be assessed, which in turn carries information about the relative spatial organization of the studied molecules or epitopes. Both uncorrected and competition-corrected transfer efficiencies were calculated to determine the apparent FRET of the dye system, while still obtaining the competition-free FRET values of a two-dye system. In our system, correcting for competition led to only minimal changes in transfer efficiency. However, in other systems closer proximity and/or larger spectral overlap between dyes could result in larger individual FRET efficiencies and therefore more significant competition, making this a valuable tool for generating FRET efficiencies comparable with values from two-dye systems.

In our experiments we used Alexa Fluor 488, Alexa Fluor 546 and Alexa Fluor 647 fluorophores as dyes A, B and C, respectively. There is sufficient spectral overlap between the excitation and emission spectra of these fluorophores to allow for all theoretically possible energy transfer routes. When measuring two-dye systems, evaluation with the classical intensity-based FRET and with the tripleFRET method gave comparable results. Also, FRET efficiencies obtained by the tripleFRET approach in three-dye systems for any dye-pair were in good agreement with the values measured and calculated for the corresponding two-dye system. However, when using the two-dye intensity-based method in a three-dye system, we measured significantly lower E_{AB} and

significantly higher E_{AC} values compared to the corresponding two-dye systems. This can be attributed to the quenching of fluorophore intensity and augmentation of sensitized emission by the third fluorophore, so that distorted values are used as acceptor and donor fluorophore intensities during energy transfer calculation.

To demonstrate the sensitivity and the discrimination power of our approach, we have mixed, in a single tube, several distinctly labeled samples and have shown that following the acquisition of a single data set it is possible to resolve the various components of the population based on the correctly calculated individual FRET efficiencies relevant to the various molecular interactions characteristic of each label type.

b) Transfer efficiency in systems with multiple transfer schemes

The results show that while our method is accurate, it fails to distinguish between different spatial distributions that produce near-identical transfer efficiency profiles. Without prior knowledge of the studied system, based solely on transfer efficiencies between pertuzumab and trastuzumab in two-dye systems, Sample 2 in Figure 11 can be assumed to follow the same spatial distribution as Sample 1. Only with the knowledge of antibody binding stochiometry (i.e. just one recognized epitope per protein) can an accurate model be constructed. Theoretically, the two cases are distinguished by a slight increase in E_{AC} and E_{BC} from the presence of additional transfer routes; however, the contribution of these routes is mostly small and can be masked by measurement noise and biological variability.

As with all ensemble-oriented methods relying on signals from several fluorophores, individual FRET processes are averaged and are indiscernible from one another (70). Sample 3 in Figure 11 demonstrates a spatial distribution where the dominant transfer processes characterized by E_{AB} and E_{AC} are competitive, and there is an independent process characterized by E_{BC}. The assumption that relay transfer is equal to the product of E_{AB} and E_{BC} is still valid; however, due to spatial separation, one of the processes contributing to relay-FRET is significantly smaller than the dominant process characterized by E_{AB} or E_{BC}. In this case, calculations assuming parallel direct and relay-FRET with the measured dominant individual transfer values will overestimate quenching of E_{AB} through dye C and contribution of relay-FRET to sensitized emission of dye C. This in turn results in underestimation of E_{AC}. If the equation set assumes only direct transfer from A to C, then E_{AB} is underestimated, E_{AC} is overestimated and relay-

FRET is neglected altogether. Ideally, the two secondary relay-FRET processes besides the dominant direct transfers should also be taken into account.

In most cases, various distinct molecular interaction schemes allow physically plausible E_{AB}, E_{AC} and E_{BC} values to be calculated from the same quenched donor and sensitized acceptor emission intensities. This in turn means that being able to calculate a given transfer efficiency does not guarantee that the FRET process is actually taking place at the molecular distance deduced. For instance, sensitized emission of dye C can be attributed to direct FRET between A and C, relay excitation through B or both. Based solely on intensity data we cannot distinguish between these cases or tell which one of them apply to a given situation. Even if multiple orientations are considered in FRET calculations, as long as the relative contribution of each to the ensemble FRET signal is not known, precise efficiency values cannot be calculated. The same effect is achieved when not all fluorophores participate in the transfer process, for instance, when three different proteins are labeled. The presence of single-dye species without transfer partners under such conditions is a problem even in traditional ensemble measurement types (71). Theoretically, an initial equation set can be developed to take multiple simultaneous distributions into account; however, the number of variables does not allow the equation set to be solved with the six measurable intensities. Therefore, accurate intensity-based calculations require prior knowledge about possible transfer routes, either from measurements in two-dye systems or known and/or limited spatial distribution of the imaged dyes (for instance rigid DNA strands that allow for only certain spatial orientations and limit the number of interacting dyes). Alternatively, single-molecule or lifetime measurements can help identify and characterize possible dye interactions in the studied system. Spectral analyses and unmixing may also be a viable route to determine the relative abundance of different dye species (52,121).

This limitation was not addressed in previous papers because the model system used to test the method ensured co-localization of all three dyes and no variation in the interaction scheme. This is an inherent property of single-molecule imaging methods, since only one fluorophore triplet and as a consequence one interaction scheme is detected at a time. Further, all measurements with DNA strands, fixed distance three-fluorophore constructs or multimers, where FRET is only possible in a given relative conformation of the imaged molecules ensured transfer processes were restricted to individual trimers of dye A, B and C. This corresponds to the scheme represented by Sample 1 in Figure 11. The key restrictions of this scheme are: FRET only takes

place within the dye-trimer; a shared dye B participates in E_{AB} and E_{BC}, so if E_{AB} and E_{BC} are detected relay-FRET also occurs and E_{AB} is quenched by E_{BC}; only dominant E_{AB} and E_{BC} contribute to relay-FRET; if E_{AC} is measured it places dyes A, B and C in the corners of a virtual triangle. In these restricted systems tripleFRET equals the efficacy of previously published three-dye methods, however without the need for an external reference sample. Whether other methods can distinguish between schemes exemplified by Samples 1 and 2 in Figure 11 or accurately measure the individual FRET efficiencies of the scheme demonstrated by Sample 3 is not known, since the model systems used to demonstrate these methods did not allow such diverse interaction schemes to occur (donor quenching methods should detect changes in total-FRET accurately). In such a fashion, either by chance or design, the restricted applicability of three-dye FRET measurements was not unmasked. It should also be noted that these considerations are only vital when precise absolute transfer efficiency values are needed and can be partially neglected when FRET is only used as a semi-quantitative indicator (e.g. identification of distinct populations, relative conformation changes) or interaction scheme changes during the experiment can be ruled out.

c) Förster distance of relay-FRET

In previous papers, the three-dye system was mostly characterized with the total energy transfer of the donor to multiple acceptors. The higher total energy transfer values of the three-dye system over a two-dye system have been interpreted as an increase in the Förster critical distance, R_0. Using equations (4) and (18), E_{relay} can be given as follows:

$$E_{relay} = \frac{1}{\left(1+\frac{r_{AB}^6}{R_{0AB}^6}\right)\left(1+\frac{r_{BC}^6}{R_{0BC}^6}\right)} = \frac{1}{\left(1+\frac{r_{ABC}^6}{R_{0ABC}^6}\right)}, \tag{49}$$

where r_{XY} is the actual physical distance of the indicated dye pair and R_{0XY} is the corresponding Förster distance. The index *ABC* denotes the distances as interpreted for the whole relay transfer process. In a three-dye system, the *AC* distance as determined through relay-FRET (which is different from the Euclidean distance between A and C, since by definition, excitation first has to travel to B before being passed on to C) is equal to the sum of *AB* and *BC* distances:

$$r_{ABC} = r_{AB} + r_{BC}\,. \tag{50}$$

By combining equations (49) and (50), the Förster critical distance for relay transfer can be given as:

$$R_{0\,ABC} = \sqrt[6]{(r_{AB} + r_{BC})^6}\,\frac{R_{0\,AB}R_{0\,BC}}{\sqrt[6]{R_{0\,AB}^6 r_{BC}^6 + R_{0\,BC}^6 r_{AB}^6 + r_{AB}^6 r_{BC}^6}} \tag{51}$$

Therefore the critical distance for relay-FRET is a function of the individual specific dye distances. Accordingly, the Förster distance calculated for relay-FRET is not an intrinsic property of the dyes determined by their spectra and quantum yields, but an arbitrary distance derived from distances calculated for two independent consecutive FRET processes. Thus in our view it is inappropriate to assign an R_0 to relay-FRET, since it is only a mathematical construct that does not have a true physical meaning, and falsely gives the impression that it possesses the same type of spatial information as the distances calculated from the individual two-dye FRET efficiencies in characterizing the three-dye system. In this sense, relay-FRET should be used as a qualitative indicator of dye interaction in three-dye systems, but not as the basis for quantitative distance measurements.

The methods and concepts presented in this thesis show, that the conventional limitations of FRET experiments can be overcome by either adding a third dye or altering the labeling ratio of the antibodies used. This allows scientists to adapt a more proactive approach and tune the behavior of the FRET system to accommodate the unique properties of the molecular system of interest. Additionally, the third dye permits investigation of higher complexity systems, since more interactions can be monitored simultaneously. In summary, tripleFRET and knowledge of the influence of dye availability further expands the capabilities of FRET measurements.

VII. Summary

We set out to characterize different F/P ratio variants of fluorophore conjugated antibodies and then utilize them to determine the effects of dye abundance on transfer efficiency. Our major results are:

- Fluorescence intensity of dye conjugated antibodies does not increase linearly with F/P ratio and dye-specific intensity saturation is present. A difference in dye behavior was also detected with anisotropy measurements.
- We showed both acceptor and donor F/P ratio directly influence the measured transfer efficiency.
- We verified that acceptor abundance has the greatest effect on FRET efficiency, with a non-linear increase in transfer efficiency due to increasing the interacting number of acceptors.
- We were able to predict dye influence with our theoretical model, which facilitates manipulation of the FRET system in a purposeful way to yield better results.

With tripleFRET, we wanted to contribute to the growing field of three-dye FRET measurements in two key areas, which are also part of the appeal of two-dye FRET: ease of use and applicability in cellular systems. Our novel three-dye method, tripleFRET has the following characteristics:

- Can be performed on regular flow cytometers.
- Allows calculation of all individual transfer efficiencies in a three-dye system without the need for an external reference sample.
- Matches the sensitivity of previous three-dye methods.
- Equals the performance of traditional two-dye FRET in two-dye systems and delivers more reliable results in three-dye systems.
- Allows direct comparison of FRET data from two- and three-dye systems when prior knowledge about the spatial localization is also available.

In conclusion, our work delivers new insights into the FRET processes in three-dye and multi-fluorophore systems. This allows us to gain additional information from the investigated system and optimize FRET measurements.

VIII. Összefoglalás

Célul tűztük ki, hogy jellemezzük a fluorofórral konjugált antitestek különböző változatait és utána segítségükkel megállapítsuk a festék kínálat hatását a transzfer hatékonyságra. A fő eredményeink:

- A festékkel konjugált antitestek fluoreszcens intenzitása nem lineárisan nő az F/P aránnyal és festékre jellemző intenzitástelítődés figyelhető meg.
- Az akceptor és donor F/P arány közvetlen hatással van a mért transzfer hatékonyságra.
- Az akceptor kínálatnak van a legnagyobb hatása a FRET hatékonyságra, a transzfer hatékonyság nem lineárisan nő a kölcsönható akceptorok számával.
- Elméleti modellünkkel meg tudtuk jósolni a festékek energiatranszferre gyakorolt hatását, ami elősegíti a FRET rendszer tudatos manipulálását a jobb eredmények érdekében.

Két kulcskérdésben, amely a két festékes FRET népszerűségéért is felelős, akartunk hozzájárulni a három festékes FRET mérések növekvő területéhez: könnyű metodika és sejtes rendszerekben való alkalmazhatóság. Az új három festékes módszerünk, a tripleFRET a következő tulajdonságokkal bír:

- Hétköznapi áramlási citométereken kivitelezhető.
- Külső referencia minta nélkül lehetővé teszi az egyedi transzfer hatékonyságok kiszámítását három festékes rendszerekben.
- Érzékenysége azonos a korábban közölt három festékes módszerekével.
- Hagyományos két festékes FRET-tel összehasonlítva két festékes rendszerben azonos eredményt nyújt, míg három festékes rendszerben megbízhatóbb.
- Lehetővé teszi a kettő és három festékes rendszerben mért transzfer hatékonyságok összevetését, ha előzőleg adatokkal rendelkezünk a térbeli pozíciókról.

Összegezve, a munkánk új adatokkal szolgál a három festékes és több fluoroféros rendszerekben lezajló FRET folyamatokról. Ez lehetővé teszi még több információ gyűjtését a vizsgált rendszerekről és a FRET mérések optimalizálását.

IX. Literature cited

1. Förster T. Zwischenmolekulare Energiewanderung und Fluoreszenz. Ann.Phys.(Leipzig) 1948;2:55-75.
2. Stryer L, Haugland RP. Energy transfer: a spectroscopic ruler. Proc Natl Acad Sci U S A 1967;58:719-26.
3. Stryer L. Fluorescence energy transfer as a spectroscopic ruler. Annu Rev Biochem 1978;47:819-46.
4. Berney C, Danuser G. FRET or no FRET: a quantitative comparison. Biophys J 2003;84:3992-4010.
5. Szollosi J, Nagy P, Sebestyen Z, Damjanovicha S, Park JW, Matyus L. Applications of fluorescence resonance energy transfer for mapping biological membranes. J Biotechnol 2002;82:251-66.
6. Jares-Erijman EA, Jovin TM. FRET imaging. Nat Biotechnol 2003;21:1387-95.
7. Kim J, Li X, Kang MS, Im KB, Genovesio A, Grailhe R. Quantification of protein interaction in living cells by two-photon spectral imaging with fluorescent protein fluorescence resonance energy transfer pair devoid of acceptor bleed-through. Cytometry A 2012;81:112-9.
8. Paar C, Paster W, Stockinger H, Schutz GJ, Sonnleitner M, Sonnleitner A. High throughput FRET screening of the plasma membrane based on TIRFM. Cytometry A 2008;73:442-50.
9. Tron L, Szollosi J, Damjanovich S, Helliwell SH, Arndt-Jovin DJ, Jovin TM. Flow cytometric measurement of fluorescence resonance energy transfer on cell surfaces. Quantitative evaluation of the transfer efficiency on a cell-by-cell basis. Biophys J 1984;45:939-46.
10. Matyus L. Fluorescence resonance energy transfer measurements on cell surfaces. A spectroscopic tool for determining protein interactions. J Photochem Photobiol B 1992;12:323-37.
11. Gordon GW, Berry G, Liang XH, Levine B, Herman B. Quantitative fluorescence resonance energy transfer measurements using fluorescence microscopy. Biophys J 1998;74:2702-13.
12. Nagy P, Vamosi G, Bodnar A, Lockett SJ, Szollosi J. Intensity-based energy transfer measurements in digital imaging microscopy. Eur Biophys J 1998;27:377-89.
13. Nagy P, Bene L, Balazs M, Hyun WC, Lockett SJ, Chiang NY, Waldman F, Feuerstein BG, Damjanovich S, Szollosi J. EGF-induced redistribution of erbB2 on breast tumor cells: flow and image cytometric energy transfer measurements. Cytometry 1998;32:120-31.
14. Sorkin A, McClure M, Huang F, Carter R. Interaction of EGF receptor and grb2 in living cells visualized by fluorescence resonance energy transfer (FRET) microscopy. Curr Biol 2000;10:1395-8.
15. Vamosi G, Damjanovich S, Szollosi J. Dissecting interacting molecular populations by FRET. Cytometry A 2008;73:681-4.
16. Szabo G, Jr., Pine PS, Weaver JL, Kasari M, Aszalos A. Epitope mapping by photobleaching fluorescence resonance energy transfer measurements using a laser scanning microscope system. Biophys J 1992;61:661-70.
17. Ivanov V, Li M, Mizuuchi K. Impact of emission anisotropy on fluorescence spectroscopy and FRET distance measurements. Biophys J 2009;97:922-9.
18. Corry B, Jayatilaka D, Rigby P. A flexible approach to the calculation of resonance energy transfer efficiency between multiple donors and acceptors in complex geometries. Biophys J 2005;89:3822-36.
19. Bader AN, Hofman EG, Voortman J, en Henegouwen PM, Gerritsen HC. Homo-FRET imaging enables quantification of protein cluster sizes with subcellular resolution. Biophys J 2009;97:2613-22.
20. Szabo A, Horvath G, Szollosi J, Nagy P. Quantitative characterization of the large-scale association of ErbB1 and ErbB2 by flow cytometric homo-FRET measurements. Biophys J 2008;95:2086-96.

21. Vamosi G, Bodnar A, Vereb G, Jenei A, Goldman CK, Langowski J, Toth K, Matyus L, Szollosi J, Waldmann TA and others. IL-2 and IL-15 receptor alpha-subunits are coexpressed in a supramolecular receptor cluster in lipid rafts of T cells. Proc Natl Acad Sci U S A 2004;101:11082-7.
22. Watrob HM, Pan CP, Barkley MD. Two-step FRET as a structural tool. J Am Chem Soc 2003;125:7336-43.
23. Zacharias DA, Violin JD, Newton AC, Tsien RY. Partitioning of lipid-modified monomeric GFPs into membrane microdomains of live cells. Science 2002;296:913-6.
24. Verveer PJ, Wouters FS, Reynolds AR, Bastiaens PI. Quantitative imaging of lateral ErbB1 receptor signal propagation in the plasma membrane. Science 2000;290:1567-70.
25. Tolar P, Sohn HW, Pierce SK. The initiation of antigen-induced B cell antigen receptor signaling viewed in living cells by fluorescence resonance energy transfer. Nat Immunol 2005;6:1168-76.
26. Glebov OO, Nichols BJ. Lipid raft proteins have a random distribution during localized activation of the T-cell receptor. Nat Cell Biol 2004;6:238-43.
27. Kim M, Carman CV, Springer TA. Bidirectional transmembrane signaling by cytoplasmic domain separation in integrins. Science 2003;301:1720-5.
28. Haitin Y, Wiener R, Shaham D, Peretz A, Cohen EB, Shamgar L, Pongs O, Hirsch JA, Attali B. Intracellular domains interactions and gated motions of I(KS) potassium channel subunits. EMBO J 2009;28:1994-2005.
29. Zhao Y, Tong C, Jiang J. Hedgehog regulates smoothened activity by inducing a conformational switch. Nature 2007;450:252-8.
30. Santoso Y, Joyce CM, Potapova O, Le Reste L, Hohlbein J, Torella JP, Grindley ND, Kapanidis AN. Conformational transitions in DNA polymerase I revealed by single-molecule FRET. Proc Natl Acad Sci U S A 2010;107:715-20.
31. Fung JJ, Deupi X, Pardo L, Yao XJ, Velez-Ruiz GA, Devree BT, Sunahara RK, Kobilka BK. Ligand-regulated oligomerization of beta(2)-adrenoceptors in a model lipid bilayer. EMBO J 2009;28:3315-28.
32. Comps-Agrar L, Kniazeff J, Norskov-Lauritsen L, Maurel D, Gassmann M, Gregor N, Prezeau L, Bettler B, Durroux T, Trinquet E and others. The oligomeric state sets GABA(B) receptor signalling efficacy. EMBO J 2011;30:2336-49.
33. Gadella TW, Jr., Jovin TM. Oligomerization of epidermal growth factor receptors on A431 cells studied by time-resolved fluorescence imaging microscopy. A stereochemical model for tyrosine kinase receptor activation. J Cell Biol 1995;129:1543-58.
34. Ng T, Squire A, Hansra G, Bornancin F, Prevostel C, Hanby A, Harris W, Barnes D, Schmidt S, Mellor H and others. Imaging protein kinase Calpha activation in cells. Science 1999;283:2085-9.
35. Gao X, Lowry PR, Zhou X, Depry C, Wei Z, Wong GW, Zhang J. PI3K/Akt signaling requires spatial compartmentalization in plasma membrane microdomains. Proc Natl Acad Sci U S A 2011;108:14509-14.
36. Janetopoulos C, Jin T, Devreotes P. Receptor-mediated activation of heterotrimeric G-proteins in living cells. Science 2001;291:2408-11.
37. Aoki K, Matsuda M. Visualization of small GTPase activity with fluorescence resonance energy transfer-based biosensors. Nat Protoc 2009;4:1623-31.
38. Yao H, Jin S. Enhancement of probe signal for screening of HIV-1 protease inhibitors in living cells. Sensors (Basel) 2012;12:16759-70.
39. Neoh SH, Brisco MJ, Firgaira FA, Trainor KJ, Turner DR, Morley AA. Rapid detection of the factor V Leiden (1691 G > A) and haemochromatosis (845 G > A) mutation by fluorescence resonance energy transfer (FRET) and real time PCR. J Clin Pathol 1999;52:766-9.
40. Emig M, Saussele S, Wittor H, Weisser A, Reiter A, Willer A, Berger U, Hehlmann R, Cross NC, Hochhaus A. Accurate and rapid analysis of residual disease in patients with CML using specific fluorescent hybridization probes for real time quantitative RT-PCR. Leukemia 1999;13:1825-32.

41. Loparev VN, McCaustland K, Holloway BP, Krause PR, Takayama M, Schmid DS. Rapid genotyping of varicella-zoster virus vaccine and wild-type strains with fluorophore-labeled hybridization probes. J Clin Microbiol 2000;38:4315-9.
42. Damjanovich S, Bene L, Matko J, Alileche A, Goldman CK, Sharrow S, Waldmann TA. Preassembly of interleukin 2 (IL-2) receptor subunits on resting Kit 225 K6 T cells and their modulation by IL-2, IL-7, and IL-15: a fluorescence resonance energy transfer study. Proc Natl Acad Sci U S A 1997;94:13134-9.
43. Jenei A, Varga S, Bene L, Matyus L, Bodnar A, Bacso Z, Pieri C, Gaspar R, Jr., Farkas T, Damjanovich S. HLA class I and II antigens are partially co-clustered in the plasma membrane of human lymphoblastoid cells. Proc Natl Acad Sci U S A 1997;94:7269-74.
44. Gaspar R, Jr., Bagossi P, Bene L, Matko J, Szollosi J, Tozser J, Fesus L, Waldmann TA, Damjanovich S. Clustering of class I HLA oligomers with CD8 and TCR: three-dimensional models based on fluorescence resonance energy transfer and crystallographic data. J Immunol 2001;166:5078-86.
45. Dornan S, Sebestyen Z, Gamble J, Nagy P, Bodnar A, Alldridge L, Doe S, Holmes N, Goff LK, Beverley P and others. Differential association of CD45 isoforms with CD4 and CD8 regulates the actions of specific pools of p56lck tyrosine kinase in T cell antigen receptor signal transduction. J Biol Chem 2002;277:1912-8.
46. Nagy P, Vereb G, Sebestyen Z, Horvath G, Lockett SJ, Damjanovich S, Park JW, Jovin TM, Szollosi J. Lipid rafts and the local density of ErbB proteins influence the biological role of homo- and heteroassociations of ErbB2. J Cell Sci 2002;115:4251-62.
47. Bagossi P, Horvath G, Vereb G, Szollosi J, Tozser J. Molecular modeling of nearly full-length ErbB2 receptor. Biophys J 2005;88:1354-63.
48. Mocanu MM, Fazekas Z, Petras M, Nagy P, Sebestyen Z, Isola J, Timar J, Park JW, Vereb G, Szollosi J. Associations of ErbB2, beta1-integrin and lipid rafts on Herceptin (Trastuzumab) resistant and sensitive tumor cell lines. Cancer Lett 2005;227:201-12.
49. Fazekas Z, Petras M, Fabian A, Palyi-Krekk Z, Nagy P, Damjanovich S, Vereb G, Szollosi J. Two-sided fluorescence resonance energy transfer for assessing molecular interactions of up to three distinct species in confocal microscopy. Cytometry A 2008;73:209-19.
50. Chen H, Puhl HL, 3rd, Koushik SV, Vogel SS, Ikeda SR. Measurement of FRET efficiency and ratio of donor to acceptor concentration in living cells. Biophys J 2006;91:L39-41.
51. Chen Y, Mauldin JP, Day RN, Periasamy A. Characterization of spectral FRET imaging microscopy for monitoring nuclear protein interactions. J Microsc 2007;228:139-52.
52. Ecker RC, de Martin R, Steiner GE, Schmid JA. Application of spectral imaging microscopy in cytomics and fluorescence resonance energy transfer (FRET) analysis. Cytometry A 2004;59:172-81.
53. Nagy P, Bene L, Hyun WC, Vereb G, Braun M, Antz C, Paysan J, Damjanovich S, Park JW, Szollsi J. Novel calibration method for flow cytometric fluorescence resonance energy transfer measurements between visible fluorescent proteins. Cytometry A 2005;67:86-96.
54. Niino Y, Hotta K, Oka K. Simultaneous live cell imaging using dual FRET sensors with a single excitation light. PLoS One 2009;4:e6036.
55. Aneja A, Mathur N, Bhatnagar PK, Mathur PC. Detection of known mutations for medical diagnostics by FRET spectroscopy. J Biomater Sci Polym Ed 2009;20:1823-30.
56. Nagy P, Szollosi J. Seeing through protein complexes by high-throughput FRET. Cytometry A 2008;73:388-9.
57. Usui K, Takahashi M, Nokihara K, Mihara H. Peptide arrays with designed alpha-helical structures for characterization of proteins from FRET fingerprint patterns. Mol Divers 2004;8:209-18.
58. van Wageningen S, Pennings AH, van der Reijden BA, Boezeman JB, de Lange F, Jansen JH. Isolation of FRET-positive cells using single 408-nm laser flow cytometry. Cytometry A 2006;69:291-8.

59. van der Meer BW. Kappa-squared: from nuisance to new sense. J Biotechnol 2002;82:181-96.
60. Turcatti G, Nemeth K, Edgerton MD, Meseth U, Talabot F, Peitsch M, Knowles J, Vogel H, Chollet A. Probing the structure and function of the tachykinin neurokinin-2 receptor through biosynthetic incorporation of fluorescent amino acids at specific sites. J Biol Chem 1996;271:19991-8.
61. Vallotton P, Tairi AP, Wohland T, Friedrich-Benet K, Pick H, Hovius R, Vogel H. Mapping the antagonist binding site of the serotonin type 3 receptor by fluorescence resonance energy transfer. Biochemistry 2001;40:12237-42.
62. Karpova TS, Baumann CT, He L, Wu X, Grammer A, Lipsky P, Hager GL, McNally JG. Fluorescence resonance energy transfer from cyan to yellow fluorescent protein detected by acceptor photobleaching using confocal microscopy and a single laser. J Microsc 2003;209:56-70.
63. Kuppig S, Nitschke R. A fusion tag enabling optical marking and tracking of proteins and cells by FRET-acceptor photobleaching. J Microsc 2006;222:15-21.
64. Verveer PJ, Rocks O, Harpur AG, Bastiaens PI. Imaging protein interactions by FRET microscopy: FRET measurements by acceptor photobleaching. CSH Protoc 2006;2006.
65. Valentin G, Verheggen C, Piolot T, Neel H, Coppey-Moisan M, Bertrand E. Photoconversion of YFP into a CFP-like species during acceptor photobleaching FRET experiments. Nat Methods 2005;2:801.
66. Zimmermann T, Rietdorf J, Girod A, Georget V, Pepperkok R. Spectral imaging and linear un-mixing enables improved FRET efficiency with a novel GFP2-YFP FRET pair. FEBS Lett 2002;531:245-9.
67. Szentesi G, Vereb G, Horvath G, Bodnar A, Fabian A, Matko J, Gaspar R, Damjanovich S, Matyus L, Jenei A. Computer program for analyzing donor photobleaching FRET image series. Cytometry A 2005;67:119-28.
68. Jurgens L, Arndt-Jovin D, Pecht I, Jovin TM. Proximity relationships between the type I receptor for Fc epsilon (Fc epsilon RI) and the mast cell function-associated antigen (MAFA) studied by donor photobleaching fluorescence resonance energy transfer microscopy. Eur J Immunol 1996;26:84-91.
69. van Munster EB, Gadella TW. Fluorescence lifetime imaging microscopy (FLIM). Adv Biochem Eng Biotechnol 2005;95:143-75.
70. Dietrich A, Buschmann V, Muller C, Sauer M. Fluorescence resonance energy transfer (FRET) and competing processes in donor-acceptor substituted DNA strands: a comparative study of ensemble and single-molecule data. J Biotechnol 2002;82:211-31.
71. Ha T, Enderle T, Ogletree DF, Chemla DS, Selvin PR, Weiss S. Probing the interaction between two single molecules: fluorescence resonance energy transfer between a single donor and a single acceptor. Proc Natl Acad Sci U S A 1996;93:6264-8.
72. Wolber PK, Hudson BS. An analytic solution to the Forster energy transfer problem in two dimensions. Biophys J 1979;28:197-210.
73. Dewey TG, Hammes GG. Calculation on fluorescence resonance energy transfer on surfaces. Biophys J 1980;32:1023-35.
74. Nazarov PV, Koehorst RB, Vos WL, Apanasovich VV, Hemminga MA. FRET study of membrane proteins: simulation-based fitting for analysis of membrane protein embedment and association. Biophys J 2006;91:454-66.
75. Koushik SV, Blank PS, Vogel SS. Anomalous surplus energy transfer observed with multiple FRET acceptors. PLoS One 2009;4:e8031.
76. Valenzuela CF, Weign P, Yguerabide J, Johnson DA. Transverse distance between the membrane and the agonist binding sites on the Torpedo acetylcholine receptor: a fluorescence study. Biophys J 1994;66:674-82.
77. Yguerabide J. Theory for establishing proximity relations in biological membranes by excitation energy transfer measurements. Biophys J 1994;66:683-93.

78. Ernst S, Duser MG, Zarrabi N, Borsch M. Three-color Forster resonance energy transfer within single F(0)F(1)-ATP synthases: monitoring elastic deformations of the rotary double motor in real time. J Biomed Opt 2012;17:011004.
79. Shyu YJ, Suarez CD, Hu CD. Visualization of AP-1 NF-kappaB ternary complexes in living cells by using a BiFC-based FRET. Proc Natl Acad Sci U S A 2008;105:151-6.
80. Ohya Y, Yabuki K, Hashimoto M, Nakajima A, Ouchi T. Multistep fluorescence resonance energy transfer in sequential chromophore array constructed on oligo-DNA assemblies. Bioconjug Chem 2003;14:1057-66.
81. Tong AK, Jockusch S, Li Z, Zhu HR, Akins DL, Turro NJ, Ju J. Triple fluorescence energy transfer in covalently trichromophore-labeled DNA. J Am Chem Soc 2001;123:12923-4.
82. Liu J, Lu Y. FRET study of a trifluorophore-labeled DNAzyme. J Am Chem Soc 2002;124:15208-16.
83. Hohng S, Joo C, Ha T. Single-molecule three-color FRET. Biophys J 2004;87:1328-37.
84. Lee S, Lee J, Hohng S. Single-molecule three-color FRET with both negligible spectral overlap and long observation time. PLoS One 2010;5:e12270.
85. Galperin E, Verkhusha VV, Sorkin A. Three-chromophore FRET microscopy to analyze multiprotein interactions in living cells. Nat Methods 2004;1:209-17.
86. He L, Wu X, Simone J, Hewgill D, Lipsky PE. Determination of tumor necrosis factor receptor-associated factor trimerization in living cells by CFP->YFP->mRFP FRET detected by flow cytometry. Nucleic Acids Res 2005;33:e61.
87. Lee NK, Kapanidis AN, Koh HR, Korlann Y, Ho SO, Kim Y, Gassman N, Kim SK, Weiss S. Three-color alternating-laser excitation of single molecules: monitoring multiple interactions and distances. Biophys J 2007;92:303-12.
88. Aneja A, Mathur N, Bhatnagar PK, Mathur PC. Triple-FRET Technique for Energy Transfer Between Conjugated Polymer and TAMRA Dye with Possible Applications in Medical Diagnostics. J Biol Phys 2008;34:487-93.
89. Navarathne D, Ner Y, Grote JG, Sotzing GA. Three dye energy transfer cascade within DNA thin films. Chem Commun (Camb) 2011;47:12125-7.
90. Kim SH, Gunther JR, Katzenellenbogen JA. Monitoring a coordinated exchange process in a four-component biological interaction system: development of a time-resolved terbium-based one-donor/three-acceptor multicolor FRET system. J Am Chem Soc 2010;132:4685-92.
91. Lee J, Lee S, Ragunathan K, Joo C, Ha T, Hohng S. Single-molecule four-color FRET. Angew Chem Int Ed Engl 2010;49:9922-5.
92. Stein IH, Steinhauer C, Tinnefeld P. Single-molecule four-color FRET visualizes energy-transfer paths on DNA origami. J Am Chem Soc 2011;133:4193-5.
93. Szentesi G, Horvath G, Bori I, Vamosi G, Szollosi J, Gaspar R, Damjanovich S, Jenei A, Matyus L. Computer program for determining fluorescence resonance energy transfer efficiency from flow cytometric data on a cell-by-cell basis. Comput Methods Programs Biomed 2004;75:201-11.
94. Roszik J, Lisboa D, Szollosi J, Vereb G. Evaluation of intensity-based ratiometric FRET in image cytometry--approaches and a software solution. Cytometry A 2009;75:761-7.
95. Vamosi G, Baudendistel N, von der Lieth CW, Szaloki N, Mocsar G, Muller G, Brazda P, Waldeck W, Damjanovich S, Langowski J and others. Conformation of the c-Fos/c-Jun complex in vivo: a combined FRET, FCCS, and MD-modeling study. Biophys J 2008;94:2859-68.
96. Friedlander E, Barok M, Szollosi J, Vereb G. ErbB-directed immunotherapy: antibodies in current practice and promising new agents. Immunol Lett 2008;116:126-40.
97. Schmitz KR, Ferguson KM. Interaction of antibodies with ErbB receptor extracellular regions. Exp Cell Res 2009;315:659-70.
98. Citri A, Yarden Y. EGF-ERBB signalling: towards the systems level. Nat Rev Mol Cell Biol 2006;7:505-16.

99. Park JG, Frucht H, LaRocca RV, Bliss DP, Jr., Kurita Y, Chen TR, Henslee JG, Trepel JB, Jensen RT, Johnson BE and others. Characteristics of cell lines established from human gastric carcinoma. Cancer Res 1990;50:2773-80.
100. Fujimoto-Ouchi K, Sekiguchi F, Yasuno H, Moriya Y, Mori K, Tanaka Y. Antitumor activity of trastuzumab in combination with chemotherapy in human gastric cancer xenograft models. Cancer Chemother Pharmacol 2007;59:795-805.
101. Craver FW, Knox RS. Theory of polarization quenching by excitation transfer. Mol. Phys. 1971;22:385-402.
102. Chan SS, Arndt-Jovin DJ, Jovin TM. Proximity of lectin receptors on the cell surface measured by fluorescence energy transfer in a flow system. J Histochem Cytochem 1979;27:56-64.
103. Gennis RB, Cantor CR. Use of nonspecific dye labeling for singlet energy-transfer measurements in complex systems. A simple model. Biochemistry 1972;11:2509-17.
104. Gombos I, Steinbach G, Pomozi I, Balogh A, Vamosi G, Gansen A, Laszlo G, Garab G, Matko J. Some new faces of membrane microdomains: a complex confocal fluorescence, differential polarization, and FCS imaging study on live immune cells. Cytometry A 2008;73:220-9.
105. Kenworthy AK, Edidin M. Distribution of a glycosylphosphatidylinositol-anchored protein at the apical surface of MDCK cells examined at a resolution of <100 A using imaging fluorescence resonance energy transfer. J Cell Biol 1998;142:69-84.
106. Szollosi J, Damjanovich S, Matyus L. Application of fluorescence resonance energy transfer in the clinical laboratory: routine and research. Cytometry 1998;34:159-79.
107. Szollosi J, Damjanovich S, Nagy P, Vereb G, Matyus L. Principles of resonance energy transfer. Curr Protoc Cytom 2006;Chapter 1:Unit1 12.
108. Zal T, Gascoigne NR. Photobleaching-corrected FRET efficiency imaging of live cells. Biophys J 2004;86:3923-39.
109. Wallrabe H, Chen Y, Periasamy A, Barroso M. Issues in confocal microscopy for quantitative FRET analysis. Microsc Res Tech 2006;69:196-206.
110. Lee NK, Kapanidis AN, Wang Y, Michalet X, Mukhopadhyay J, Ebright RH, Weiss S. Accurate FRET measurements within single diffusing biomolecules using alternating-laser excitation. Biophys J 2005;88:2939-53.
111. Munoz-Losa A, Curutchet C, Krueger BP, Hartsell LR, Mennucci B. Fretting about FRET: failure of the ideal dipole approximation. Biophys J 2009;96:4779-88.
112. Wang YL. Noise-induced systematic errors in ratio imaging: serious artefacts and correction with multi-resolution denoising. J Microsc 2007;228:123-31.
113. Gautier I, Tramier M, Durieux C, Coppey J, Pansu RB, Nicolas JC, Kemnitz K, Coppey-Moisan M. Homo-FRET microscopy in living cells to measure monomer-dimer transition of GFP-tagged proteins. Biophys J 2001;80:3000-8.
114. Altman D, Goswami D, Hasson T, Spudich JA, Mayor S. Precise positioning of myosin VI on endocytic vesicles in vivo. PLoS Biol 2007;5:e210.
115. Robia SL, Flohr NC, Thomas DD. Phospholamban pentamer quaternary conformation determined by in-gel fluorescence anisotropy. Biochemistry 2005;44:4302-11.
116. Vaknin A, Berg HC. Osmotic stress mechanically perturbs chemoreceptors in Escherichia coli. Proc Natl Acad Sci U S A 2006;103:592-6.
117. Matyus L, Szollosi J, Jenei A. Steady-state fluorescence quenching applications for studying protein structure and dynamics. J Photochem Photobiol B 2006;83:223-36.
118. Maliwal BP, Raut S, Fudala R, D'Auria S, Marzullo VM, Luini A, Gryczynski I, Gryczynski Z. Extending Forster resonance energy transfer measurements beyond 100 A using common organic fluorophores: enhanced transfer in the presence of multiple acceptors. J Biomed Opt 2012;17:011006.
119. Lopez-Gimenez JF, Canals M, Pediani JD, Milligan G. The alpha1b-adrenoceptor exists as a higher-order oligomer: effective oligomerization is required for receptor maturation, surface delivery, and function. Mol Pharmacol 2007;71:1015-29.

120. Milligan G, Pediani JD, Canals M, Lopez-Gimenez JF. Oligomeric structure of the alpha1b-adrenoceptor: comparisons with rhodopsin. Vision Res 2006;46:4434-41.
121. Sun Y, Wallrabe H, Booker CF, Day RN, Periasamy A. Three-color spectral FRET microscopy localizes three interacting proteins in living cells. Biophys J 2010;99:1274-83.
122. Klostermeier D, Sears P, Wong CH, Millar DP, Williamson JR. A three-fluorophore FRET assay for high-throughput screening of small-molecule inhibitors of ribosome assembly. Nucleic Acids Res 2004;32:2707-15.
123. He L, Olson DP, Wu X, Karpova TS, McNally JG, Lipsky PE. A flow cytometric method to detect protein-protein interaction in living cells by directly visualizing donor fluorophore quenching during CFP-->YFP fluorescence resonance energy transfer (FRET). Cytometry A 2003;55:71-85.
124. Goedhart J, van Weeren L, Adjobo-Hermans MJ, Elzenaar I, Hink MA, Gadella TW, Jr. Quantitative co-expression of proteins at the single cell level--application to a multimeric FRET sensor. PLoS One 2011;6:e27321.

Register Number: DEENKÉTK/125/2013.
Item Number:
Subject: Ph.D. List of Publications

Candidate: Ákos Fábián

Neptun ID: V2H8VR

Doctoral School: Doctoral School of Molecular Medicine

List of publications related to the dissertation

1. **Fábián, Á.**, Horváth, G., Vámosi, G., jr. Vereb, G., Szöllősi, J.: TripleFRET measurements in flow cytometry.
   Cytom. Part A. 83 (4), 375-385, 2013.
   DOI: http://dx.doi.org/10.1002/cyto.a.22267
   IF:3.729 (2011)

2. **Fábián, Á.I.**, Rente, T., Szöllősi, J., Mátyus, L., Jenei, A.: Strength in numbers: Effects of Acceptor Abundance on FRET Efficiency.
   Chemphyschem. 11 (17), 3713-3721, 2010.
   DOI: http://dx.doi.org/10.1002/cphc.201000568
   IF:3.339

List of other publications

3. **Fábián, Á.**, jr. Vereb, G., Szöllősi, J.: The hitchhikers guide to cancer stem cell theory: Markers, pathways and therapy.
   Cytom. Part A. 83A (1), 62-71, 2012.
   DOI: http://dx.doi.org/10.1002/cyto.a.22206
   IF:3.729 (2011)

4. **Fábián, Á.**, Barok, M., jr. Vereb, G., Szöllősi, J.: Die Hard: Are cancer stem cells the Bruce Willises of tumor biology?
   Cytometry A. 75A (1), 67-74, 2009.
   DOI: http://dx.doi.org/10.1002/cyto.a.20690
   IF:3.032

5. Varga, Z., Csépány, T., Papp, F., **Fábián, Á.**, Gogolák, P., Tóth, Á., Panyi, G.: Potassium channel expression in human CD4(+) regulatory and naive T cells from healthy subjects and multiple sclerosis patients.
Immunol. Lett. 124 (2), 95-101, 2009.
DOI: http://dx.doi.org/10.1016/j.imlet.2009.04.008
IF:2.906

6. Fazekas, Z., Petrás, M., **Fábián, Á.**, Pályi-Krekk, Z., Nagy, P., Damjanovich, S., jr. Vereb, G., Szöllősi, J.: Two-sided fluorescence resonance energy transfer for assessing molecular interactions of up to three distinct species in confocal microscopy.
Cytom. Part A. 73 (3), 209-219, 2008.
DOI: http://dx.doi.org/10.1002/cyto.a.20489
IF:3.259

7. Kovács, T., Békési, G., **Fábián, Á.**, Rákosy, Z., Horváth, G., Mátyus, L., Balázs, M., Jenei, A.: DNA flow cytometry of human spermatozoa: Consistent stoichiometric staining of sperm DNA using a novel decondensation protocol.
Cytometry A. 73 (10), 965-970, 2008.
DOI: http://dx.doi.org/10.1002/cyto.a.20618
IF:3.259

8. jr. Sipka, S., Bráth, E., Tóth F., F., Aleksza, M., Kulcsár, A., **Fábián, Á.**, Baráth, S., Balogh, P., Sipka, S., Furka, I., Mikó, I.: Cellular and serological changes in the peripheral blood of splenectomized and spleen autotransplanted mice.
Transpl. Immunol. 16 (2), 99-104, 2006.
DOI: http://dx.doi.org/10.1016/j.trim.2006.03.013
IF:2.297

9. jr. Sipka, S., Bráth, E., Tóth F., F., **Fábián, Á.**, Sipka, S., Németh, N., Bálint, A., Furka, I., Mikó, I.: Distribution of peripheral blood cells in mice after splenectomy or autotransplantation.
Microsurgery. 26 (1), 43-49, 2006.
DOI: http://dx.doi.org/10.1002/micr.20209
IF:0.882

10. Horváth, G., Petrás, M., Szentesi, G., **Fábián, Á.**, Park, J.W., jr. Vereb, G., Szöllősi, J.: Selecting the right fluorophores and flow cytometer for fluorescence resonance energy transfer measurements.
Cytometry A. 65A (2), 148-157, 2005.
DOI: http://dx.doi.org/10.1002/cyto.a.20142
IF:2.115

11. ifj Sipka S., Bráth E., Tóth F. F., **Fábián Á.**, Furka I., Mikó I.: Lép autotransplantatio és lépeltávolítás haematologiai és immunologiai hatásainak összehasonlító vizsgálata egerekben.
Magyar Seb. 58, 84-88, 2005.

12. Szentesi, G., jr. Vereb, G., Horváth, G., Bodnár, A., **Fábián, Á.**, Matkó, J., Gáspár, R., Damjanovich, S., Mátyus, L., Jenei, A.: Computer program for analyzing donor photobleaching FRET image series.
Cytometry A. 67 (2), 119-128, 2005.
DOI: http://dx.doi.org/10.1002/cyto.a.20175
IF:2.115

Total IF: 30.662

Total IF (publications related to the dissertation): 7.068

The Candidate's publication data submitted to the Publication Database of the University of Debrecen have been validated by Kenezy Life Sciences Library on the basis of Web of Science, Scopus and Journal Citation Report (Impact Factor) databases.

29 March, 2013

X. Key words

Fluorescence resonance energy transfer

FRET

Flow cytometry

Acceptor

Donor

Three-dye FRET

Multi-fluorophore FRET

Inter-dye distance

XI. Acknowledgements

I would first like to thank my lovely wife Mariann for being both inspiration and motivation in everything I do.

I would like to thank my parents and family for their support and love. You taught me integrity, perseverance and passion, for this I am forever grateful.

I would like to thank Dr. Szöllősi János for being a mentor over all these years. Thank you for your guidance and for knowing when to trust my decisions and when to question them.

Thank you to Dr. Horváth Gábor and Dr. Vereb György Jr. for all they have taught me, whether through critique or advice. If there ever was a question that you couldn't answer, it sure wasn't for a lack of trying.

A would like to acknowledge the help and assistance of Dr. Jenei Attila and Dr. Vámosi György. Thank you to Rente Tünde for her contribution to my work.

Additionally thank you to all present and past colleagues of the Biophysics and Cell Biology Department for creating a friendly environment. It was a joy to work with you all. Dr. Barok Márk, Dr. Petrás Miklós, Dr. Pályiné Krekk Zsuzsa, Juhász Judit, Dr. Fazekas Zsolt, Dr. Horváth Gábor and Dr. Sebestyén Zsolt, the experience of sharing a room with you remains unforgettable.

Last, but not least, I must thank two teachers, who had a great impact on me long before I knew what a flow cytometer is. First Bíró Lajos, who laid the foundations for, as my wife puts it, being able to solve equations for pages without actually ever using a number. Second, a very special thank you to Dr. Szegedi Ervin for igniting and nurturing my interest in physics. I feel privileged that you were my teacher.

Experimental work was performed with the support of the TÁMOP-4.2.2.A-11/1/KONV-2012-0025 project. The doctoral training program was supported by the TÁMOP-4.2.2/B-10/1-2010-0024 project. The projects are co-financed by the European Union and the European Social Fund.

XII. Appendix – Publications related to the dissertation